nature communications

Article

https://doi.org/10.1038/s41467-024-54470-0

Re-localization of a repeat-containing fungal effector by apoplastic protein Chitinase-like 1 blocks its toxicity

Received: 13 November 2023

Accepted: 8 November 2024

Published online: 22 November 2024

Check for updates

Hanqiao Liu[1,2], Wenshu Zhang[1,2], Qinqfei He[1,2], Reyila Aikemu[1,2], Huijuan Xu[1,2], Zhan Guo[1,2], Lu Wang[1,2], Weixi Li[1,2], Guilin Wang[1,2], Xinyu Wang[2,3] ✉ & Wangzhen Guo[1,2] ✉

A fungal effector that is toxic to plant cells was identified in *Verticillium dahliae*. The effector contains a non-canonical Common in several Fungal Extracellular Membrane proteins (CFEM) domain, a tandem repeat region consisting of four 14-amino acid repeats rich in proline, and a C-terminal region, thus is designated *V. dahliae* tetrapeptide repeat protein (VdTRP). The membrane targeting of VdTRP is vital for its cell toxicity. CFEM mediates the membrane targeting and the tandem repeat region exerts the toxic function upon cell membrane. The chitinase-like 1 (CTL1), an essential apoplastic protein of cotton, can redirect VdTRP from cell membrane to apoplast. Transgenic cotton overexpressing *CTL1* greatly enhances cotton resistance to *V. dahliae* without affecting cotton growth and development, implicating its potential application in breeding cotton with high wilt resistance. Our data demonstrates that genetic manipulation of effector target constitutes potential strategy for improving crop resistance to fungal pathogens.

Plant pathogenic fungi represent the largest group of disease-causing agents on crop plants, and are a constant and major threat to agriculture worldwide. In 2022, the Food and Agricultural Organization (FAO) of the United Nations reported that 168 crops are affected by hundreds of fungal diseases. Despite widespread use of fungicide and planting of cultivars with more disease resilient, growers worldwide lose between 10% and 23% of their crops due to fungal disease each year[1].

To promote colonization and infection of host plant, pathogenic fungi produce a large number of effector molecules to modulate host physiology or evade recognition by host cells[2–5]. In contrast to bacterial effectors that are injected into plant cells by type III secretion system, many fungal effectors functions in the apoplast of plant cells, and others may enter into plant cells by host uptake machinery and target to various cell compartment and play a role therein[6,7]. Effectors of biotrophic fungal pathogens are often used to inhibit host defense and host cell death to facilitate acquire nutrition from living cells; effectors of necrotrophic pathogenic fungi are often used to kill host cells and obtain nutrition from dead cells[8]. In contrast, hemi-biotrophic fungi produce both type of effectors in different infection stages, adding complexities to pathogenesis.

During evolution, plant have evolved complex defense strategies to combat pathogenic fungi with different life styles[9–12]. PTI (pattern-triggered immunity) and ETI (effector-triggered immunity) are developed to effectively defend against biotrophic fungal pathogens, whereas, they may be not effective to defend against necrotrophic fungal pathogens. In particular, some "resistance proteins" mediating cell death can function as susceptible genes and favor infection by necrotrophs[13,14]. In several cases, it is not the traditional "resistance proteins" but are certain enzymes that effectively reduce the virulence of this kind of fungal pathogens[15,16]. How plants combat hemi-biotrophs are complex and are still elusive.

Although the functions of most bacterial effectors are known, the roles of fungal effectors are under exploring. In recent years, the study of these effectors has expanded our knowledge on understanding the

[1]State Key Laboratory of Crop Genetics & Germplasm Enhancement and Utilization, Nanjing Agricultural University, Nanjing 210095, China. [2]Engineering Research Center of Ministry of Education for Cotton Germplasm Enhancement and Application, Nanjing Agricultural University, Nanjing 210095, China. [3]College of Life Sciences, Nanjing Agricultural University, Nanjing 210095, China. ✉e-mail: xywang@njau.edu.cn; moelab@njau.edu.cn

molecular basis of pathogenesis. In addition, fungal effectors are emerging as tools to accelerate disease resistance breeding of crops[17,18]. In fact, in some plant pathosystem, they have been used in effector-assisted resistance gene cloning, identification of resistance resources and deployment cultivars[19].

Verticillium dahliae is a hemibiotrophic soilborne fungal pathogen and can infect a wide range of plant species, including cotton. It infects plant through the roots and thrives in vascular systems, resulting in wilting symptoms in host. The Verticillium wilt of cotton results in huge yield losses in cotton growing areas each year. Fungicide is not effective to manage the disease and breeding resistance cultivars become an economic approach. Unfortunately, germplasms with high wilt resistance are not found in cotton (*Gossypium hirsutum*), which accounts for more than 90% of the world's total cotton output. In such situation, genetic engineering maybe an alternative to improve cotton resistance to this disease. To achieve this, the key is to find proper target gene suitable for this manipulation. In recent years, genetic modification the effector target has shed light on the improvement of plant resistance. For instances, gene-editing the susceptible genes[20], modification the promoter of target genes[21], and overexpression of target genes are reported to be effective approaches to improve crop resistance[22].

Here, we report the identification of an effector protein in *V. dahliae*. This effector contains a cell death-inducing repeat domain, and exerts its function by targeting on plasma membrane of plant cells through a N-terminal non-canonical CFEM domain. We found that an apoplastic protein, named the chitinase-like 1 (CTL1), can interact with the effector and eliminate its cell toxicity, and that transgenic cotton overexpressing *CTL1* greatly enhances the wilt resistance of cotton. In addition, *CTL1* knocking down seriously affects cotton growth and development, suggesting that CTL1 is essential in cotton. Our data indicate that change the expression of an essential gene can improve cotton resistance to the wilt disease. This study and a recent report[22] represent strategies to improve crop resistance to the hemibiotrophic fungal pathogen.

Results

VdTRP may constitute a protein toxin in *V. dahliae*

V. dahliae is estimated to encode more than 700 secreted effector proteins[23]. Although some of these were functionally studied, much of them are still unexplored. To identify key virulence effectors in cotton pathogenic *V. dahliae*, we performed a global gene expression profiling in spores of *V. dahliae* strain V991 following root induction by RNA-seq assays. This analysis generated a total of 976 genes that were responsive to root induction compared with controls. Among these, 156 genes with FPKM (Fragments Per Kilobase of exon model per Million mapped fragments) values greater than 300 were selected and used for prediction the presence of potential signal peptide in the encoding proteins. A total of 23 proteins were identified having the predicted signal peptide (Supplementary Table 1). One protein raised our special concerns because its expression is responsive to root induction, and of note, it results in severe and fast cell and tissue death when analyzed by agroinfiltration in *N. benthamiana* leaves (Fig. 1a, b, d). The protein encodes 196 amino acids with 14 cysteine residues that are evenly distributed in the N-terminus and the central region (Fig. 1c). Protein Blast in NCBI reveal that it is an uncharacterized protein with no known domains. We then investigated the three-dimentional (3D) structural information of the protein in SWISS-MODEL and by AlphaFold. Although the two approaches could not generate reliable models or models of the whole protein, both predicted that there exists a CFEM domain in the N-terminus, which forms three α-helices (Fig. 1c and Supplementary Fig. 1a–c). Moreover, by detailed survey of the protein sequence, we identified a specific IPGGCNPAHPGSCP motif which has been tandemly repeated four times in the central region of the effector protein, thus the protein is designated *V. dahliae* tetrapeptide tandem repeat protein (VdTRP). Furthermore, we found that the 14-residue repeat motif is rich in proline (having four proline in each motif), thus the repeat domain constitutes a member of the proline-rich motif (Fig. 1c).

To further characterize the cell death-inducing ability of VdTRP, we transiently expressed VdTRP in cotton cotyledons and in leaves of Arabidopsis by agroinfiltration. A construct harboring *VdTRP-3×FLAG-RFP* could reproducibly induce cell death in cotton and Arabidopsis besides in *N. benthamiana* (Fig.1e, f). We observed that VdTRP seems cause an uncontrolled, severe and fast cell and tissue death, a phenotype similar as VdNLP1 toxin[24,25], we consider that VdTRP may constitute a member of protein toxins in *V. dahliae*.

To investigate whether VdTRP is required for *V. dahliae* infection of host plants, we generated VdTRP knockout mutant strain △*vdtrp* in V991 background and the complemented strain △*vdtrp/ VdTRP* (Supplementary Fig. 1d, e). Infection assays showed that △*vdtrp* strain displayed significantly reduced virulence on cotton plants, as was revealed by the decreased percentage of wilted leaves, the degree of vascular discoloration and the relative fungal biomass in △*vdtrp* infected cotton plants compared with that wildtype stain V991 and △*vdtrp/ VdTRP* infected cotton plants (Fig. 1g, h and Supplementary Fig. 2a–c). Together, we identify that VdTRP may constitute a member of protein toxins in *V. dahliae*, which induces severe cell and tissue death and is required for *V. dahliae* infection of cotton plants.

Both CFEM and the repeat domain is required for VdTRP cell toxicity

Previous studies have shown that CFEM and the repeat domains play vital roles in virulence of fungal effectors[26,27], we thus investigated the contributions of the two domains to VdTRP virulence. To this end, we generated a series of constructs for agroinfiltration assays, including the CFEM deletion mutant, and five different repeat motif or C-terminus truncated versions (Fig. 2a). Transient expression of these constructs in *N. benthamiana* leaves by agroinfiltration demonstrated that deletion of CFEM significantly reduced the virulence of VdTRP even in presence of the repeat domain (Fig. 2b and Supplementary Fig. 3a), while deletion of the four repeat domain completely abolished effector virulence even in presence of CFEM domain (Fig. 2c and Supplementary Fig. 3b). In addition, we observed a positive correlation between the severity of cell death and the number of the repeat motif present in respective mutant effectors (Fig. 2c, Supplementary Fig. 3c). The protein expression in *N. benthamiana* for each construct was verified using anti-FLAG immunoblotting (Fig. 2d, e), and the extent of cell death caused by each construct was quantified by measuring ion leakage. Transient expression of full-length VdTRP resulted in severe ion leakage and cytolysis in plant cells, whereas deletion of CFEM or the repeat domain significantly reduced the effects (Fig. 2f, g). Based on our data we conclude that both CFEM and the repeat domain is required for full virulence of VdTRP, and the repeat domain is responsible for cell toxicity but requires the CFEM domain. Since proline is a very unusual amino acid and greatly affects protein structure and function, we therefore determined its role in effector virulence. We generated a VdTRP variant in which all the proline residues in the repeat motif were mutated to alanine (Fig. 2h). The virulence of the VdTRP variant was investigated by transient expression in *N. benthamiana* by agroinfiltration. Results showed that the virulence of VdTRP variant was completely abolished, as revealed by the loss of cell death phenotype and similar level of ion leakage with the control (Fig. 2i, j and Supplementary Fig. 3d). Thus, the proline residues play vital roles in the virulence of the repeat motif/repeat domain upon plasma membrane.

To further characterize the toxicity of VdTRP and its various mutant proteins to cells/ cell membranes, we investigated the responses of Arabidopsis protoplast to treatment by these proteins. *E. coli* expressed proteins of a series constructs were used to treat Arabidopsis protoplast (Supplementary Fig. 4a). We observed that VdTRP

https://doi.org/10.1038/s41467-024-54470-0

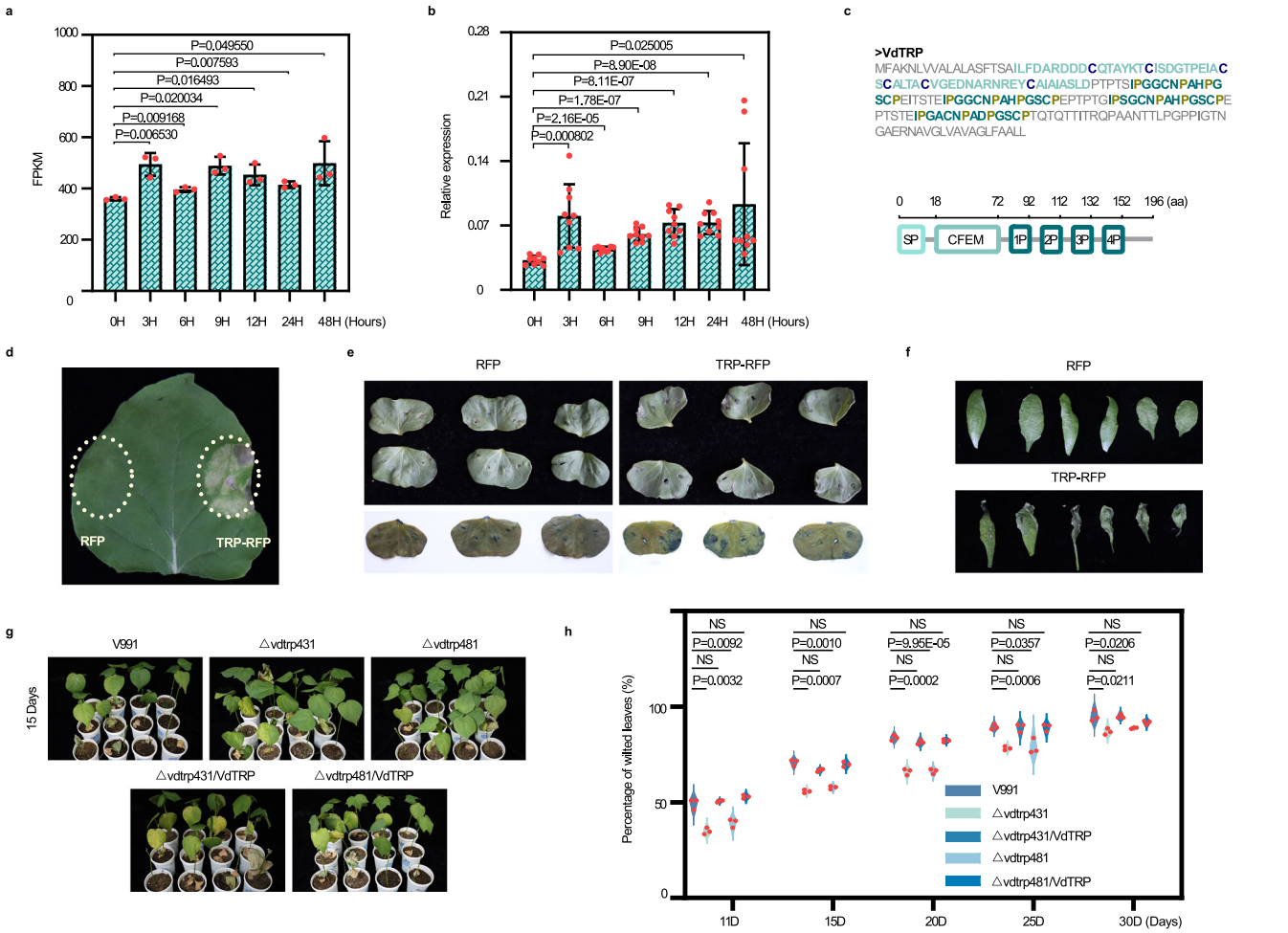

Fig. 1 | VdTRP is a repeat-containing protein toxin of *V. dahliae*. **a** Expression patterns of *VdTRP* in spores of *V. dahliae* strain V991 upon cotton root induction at 0, 3, 6, 9, 12, 24, and 48 h. The expression data were converted to FPKM to calculate the expression levels of *VdTRP*. Data are shown as mean ± s.d. (n = 3 biologically independent experiments). **b** *VdTRP* expression in spores of *V. dahliae* strain V991 was quantified by RT-qPCR. *β-tubulin* (KF555285.1) gene was used as internal control. Data are shown as mean ± s.d. (n = 9 biologically independent experiments). **c** Protein sequence and schematic overview of the VdTRP protein showing different domains. The amino acids shown in light green represent the CFEM domain, with cysteine residues highlighted in purple, and amino acids shown in dark green represent the tetrapeptide repeat domain, with proline highlighted in yellow. VdTRP can induce the cell death in leaves of *N. benthamiana* (**d**), cotyledons of cotton (**e**), and leaves of Arabidopsis (**f**). Trypan blue staining indicates the degree of cell death. RFP, red fluorescent protein. VdTRP shortens as TRP. **g** The *Δvdtrp* mutant displays reduced virulence in cotton plants. Photographs were taken after 15 days post inoculation by *V. dahliae*. **h** Percentage of wilted cotton leaves inoculated with wild type *V. dahliae* strain *V991*, two *VdTRP* knockout mutants *Δvdtrp431*, *Δvdtrp481* and the complemented strains *Δvdtrp431/VdTRP*, *Δvdtrp481/VdTRP*, respectively. The points represent three biological repeats (n = 3). Each biological repeat contains 10 seedlings. All statistical analyses were performed by the two-tailed Student's t test. NS no significance. Source data are provided as a Source Data file.

could rapidly induce cell death (Supplementary Movie 1, 2). Statistical analysis reveal that the extent of cell death positively correlates with the copies of the repeat motif present in expressed proteins, and that the toxicity of VdTRP$^{P/A}$ mutant is at similar levels as the mock, the empty vector controls His-GST, and the repeat domain deletion mutant His-GST-TRP$^{1-75}$(Supplementary Fig. 4b).

Since the type of cell death induced by VdTRP is similar to that of VdNLP1, we ask whether VdTRP exerts its virulence function through targeting plasma membranes. To answer this question, we investigated the subcellular localization of VdTRP. Transient expression of VdTPR-GFP construct in *N. benthamiana* showed that VdTRP-GFP overlapped with a membrane marker protein AtPIP2A fused with RFP, demonstrating that VdTRP can target plasma membrane (Fig. 3a, b). To determine which domain are involved in VdTPR membrane targeting, we generated VdTRP mutants in which CFEM, repeat domain and the C-terminus were respectively deleted. Subcellular localization assays revealed that CFEM deletion but not the other two domains affected VdTRP membrane targeting (Fig. 3c–e). To investigate the potential lipids that might mediate VdTRP membrane targeting, we performed lipid-protein interaction assays. Several constructs, including His-GST-TRP, His-GST-TRP$^{\Delta CFEM}$, and His-GST-TRP$^{(P/A)}$ were expressed in *E. coli* and purified proteins were subjected to lipid binding assay (Fig. 3g). The results reveal that wild-type VdTRP protein has high affinity with phosphatidylserine and has weak binding with Ptdins(5)P (Fig. 3h). While deletion of CFEM completely abolishes this binding property (Fig. 3h). Interestingly, VdTRP variant in which all prolines in the repeat domain were mutated to alanine could bind several lipids including phosphatidylserine (Fig. 3h). Our data suggests that VdTRP membrane targeting are mediated by CFEM through strong binding with phosphatidylserine. Since CFEM deletion seriously affected VdTRP virulence, we conclude that membrane targeting through CFEM is vital for VdTRP full virulence.

VdTRP forms pores in lipid membranes and leads to rapid mammalian cell death

Since many toxins exert their functions by forming pores on cell membrane, we investigate whether VdTRP might behave similarly. To this end, we investigated cell topography and surface charge

https://doi.org/10.1038/s41467-024-54470-0

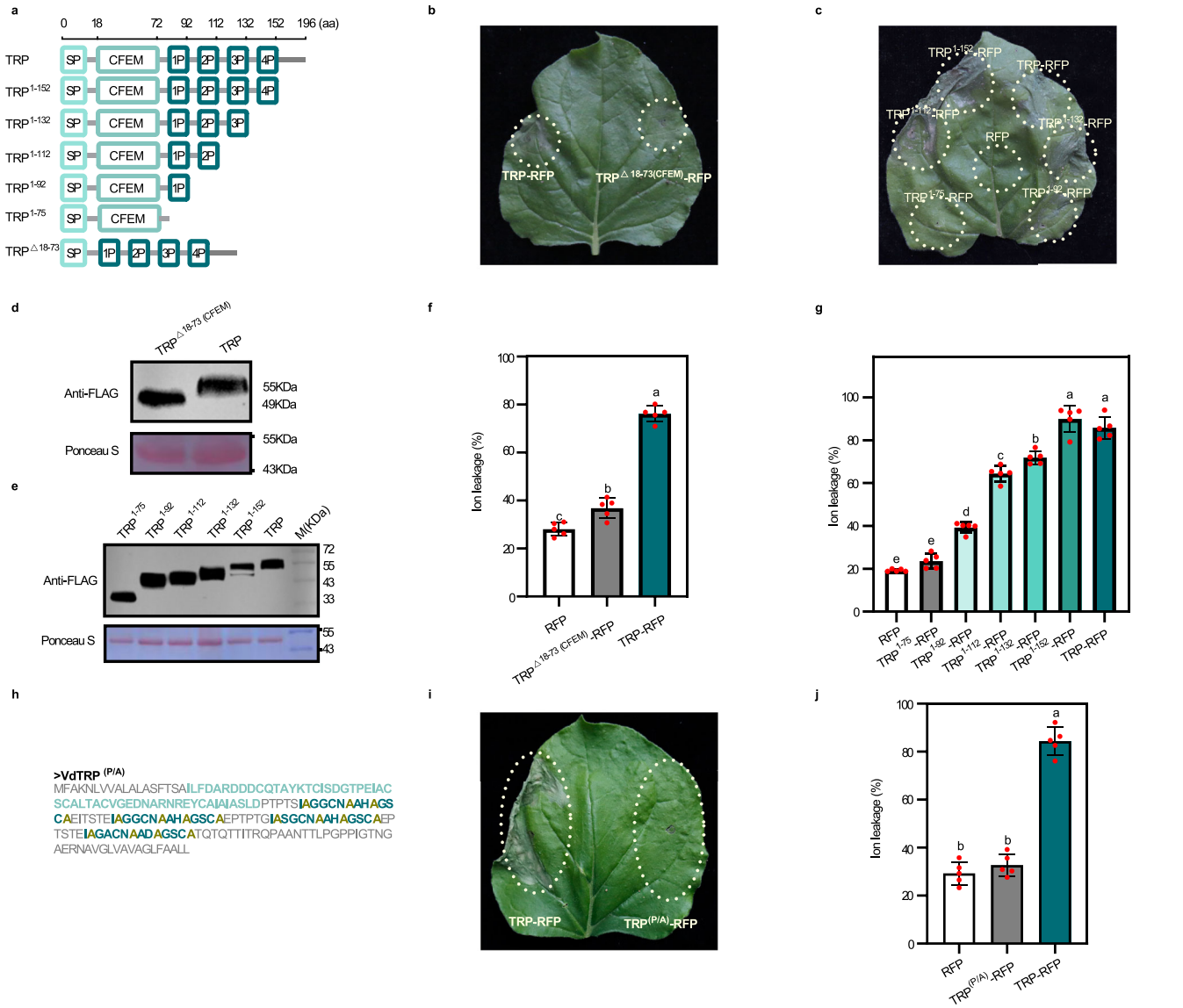

Fig. 2 | Both CFEM and the repeat domain is required for VdTRP cell toxicity. **a** Schematic diagram of the full-length VdTRP and six different truncated versions. **b** CFEM domain is required for VdTRP cell toxicity. **c** Virulence test for repeat domains with five different truncated versions. Empty vector with a red fluorescence protein (RFP) was used as the negative control. **d**, **e** Confirmation of protein expression for each construct in **b** and **c** by western blot with anti-FLAG. Proteins stained with Ponceau S serve as a total protein loading control. The experiment was independently repeated three times with similar results. **f**, **g** Degree of cell death in **b** and **c** were determined by ion leakage assays, respectively. **h** Diagram of the VdTRP variant in which all the proline residues in the repeat motif were mutated to alanine. **i** VdTRP $^{P/A}$ variant completely lost cell toxicity. **j** Degree of cell death in **j** was determined by ion leakage assays. Data in **f**, **g** and **j** are shown as mean ± s.d. (n = 5 biologically independent experiments), different letters denote significant differences ($p < 0.05$) by one-way ANOVA with Duncan's multiple range tests. VdTRP shortens as TRP. Source data are provided as a Source Data file.

changes caused by VdTRP treatment using scanning ion conductance microscopy (SICM). This technique requires cells to be adhered to culture dishes, so we used cultured mammalian cells to do the experiment. Here we used rat cardiomyocyte cells as the cell model to investigate the toxic effects of VdTRP protein on cells. These cells can adhere to culture dishes, making investigation using SICM operational. Furthermore, live rat cardiomyocyte cells exhibit wedge-shaped morphology while dead cells become round, making observation easy by optical microscope. We first observed the effects of VdTRP treatment on growing of rat cardiomyocytes under optical microscope. As shown in Fig. 4a, in mock and empty vector control His-GST, cells grew well and appeared as wedge shape. In contrast, VdTRP treatment for only 2 min, a large number of round cells were observed under optical microscope. Statistical analysis reveals that VdTRP protein treatment leads to about 48.5% cell death compared with the non-treatment controls (Fig. 4b). We then used SICM to study 2D and enhanced color topography (obtained by using the height difference of adjacent pixels to enhance the height contrast of the topography) images and cell surface charge variations in rat cardiomyocytes cells with or without VdTRP protein treatment (Fig. 4c, d). The ΔI-SICM method was used to monitor cell membrane damages in rat cardiomyocyte cells upon VdTRP treatment[28]. As shown in Fig. 4e–g, compared with the non-treatment control cells (Fig. 4e, without VdTRP protein treatment), clear pores were detected on cell surface in some VdTRP protein-treated cells (Fig. 4f). These cells might be at the early stage of membrane damage. In other cells, the integrity of cell membrane was seriously disrupted and became shrinking (Fig. 4g). Intriguingly, compared to the control (Fig. 4h), we were able to detect large surface charge variations in cells of early stage of membrane

https://doi.org/10.1038/s41467-024-54470-0

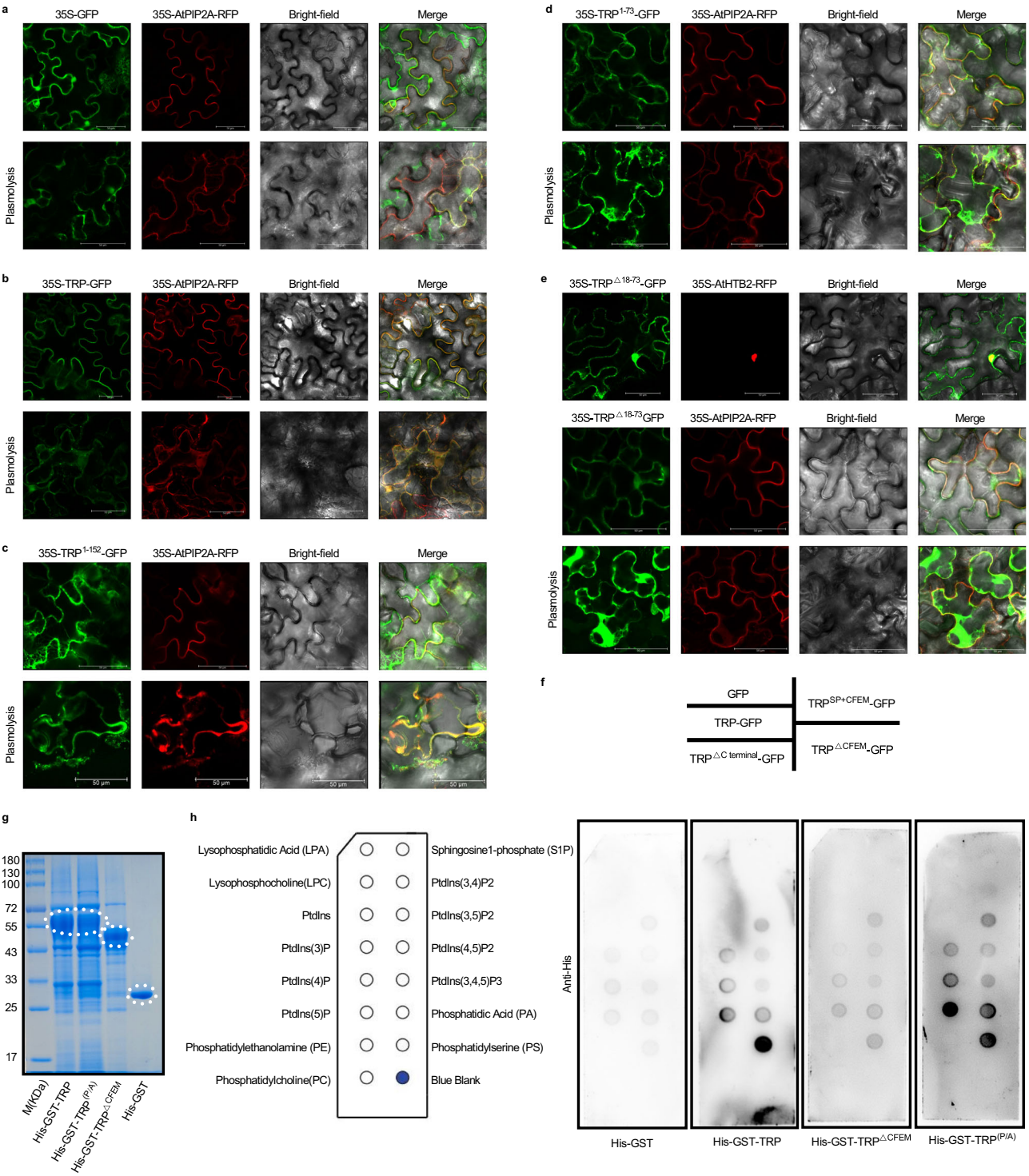

Fig. 3 | The CFEM domain is required for VdTRP plasma membrane targeting. **a**–**e** TRP-GFP (**b**), TRP$^{\triangle C\text{-terminal}}$-GFP (**c**), and TRP$^{SP+CFEM}$-GFP (**d**) colocalize with cell membrane marker AtPIP2A-RFP, either before or after plasmolysis. To induce plasmolysis, *N. benthamiana* leaves were immersed in a 0.8 M mannitol solution for one hour. TRP$^{\triangle CFEM}$-GFP (**e**) colocalizes with nuclear marker AtHTB2-RFP. After plasmolysis, TRP$^{\triangle CFEM}$-GFP signals are largely distributed in cytoplasm, with a small part in microdomains of cell membrane. 35S-GFP as positive control (**a**). Scale bars: 50 μm. **f** Indications of the respective figure showing which construct is used to perform localization experiment. **g**, **h** TRP strongly bind phosphatidylserine in a protein-lipid interaction assay. Deletion of CFEM abolishes this specific binding. Several constructs including His-GST-TRP, His-GST-TRP$^{\triangle CFEM}$ and His-GST-TRP $^{P/A}$ were *E. coli* expressed respectively and each purified protein were used in protein-lipid binding. His-GST was used as the negative control. The dash circles represent the purified target protein in **g**. GFP, green fluorescent protein. RFP red fluorescent protein. VdTRP shortens as TRP. The experiment was independently repeated three times with similar results (**a**–**e**, **h**). Source data are provided as a Source Data file.

damage (Fig. 4i), however, low surface charge variations could be detected in cells displaying severe membrane damage, as shown by many blue points (Fig. 4j). This maybe that at later stages of membrane damage, cells became fully permeable and no large charge variations existed on cell surface. Based on these data, we propose that VdTRP protein can seriously disrupt the integrity of cell membrane by forming pores on cell surface, leading to severe cell permeability and rapid cell death.

https://doi.org/10.1038/s41467-024-54470-0

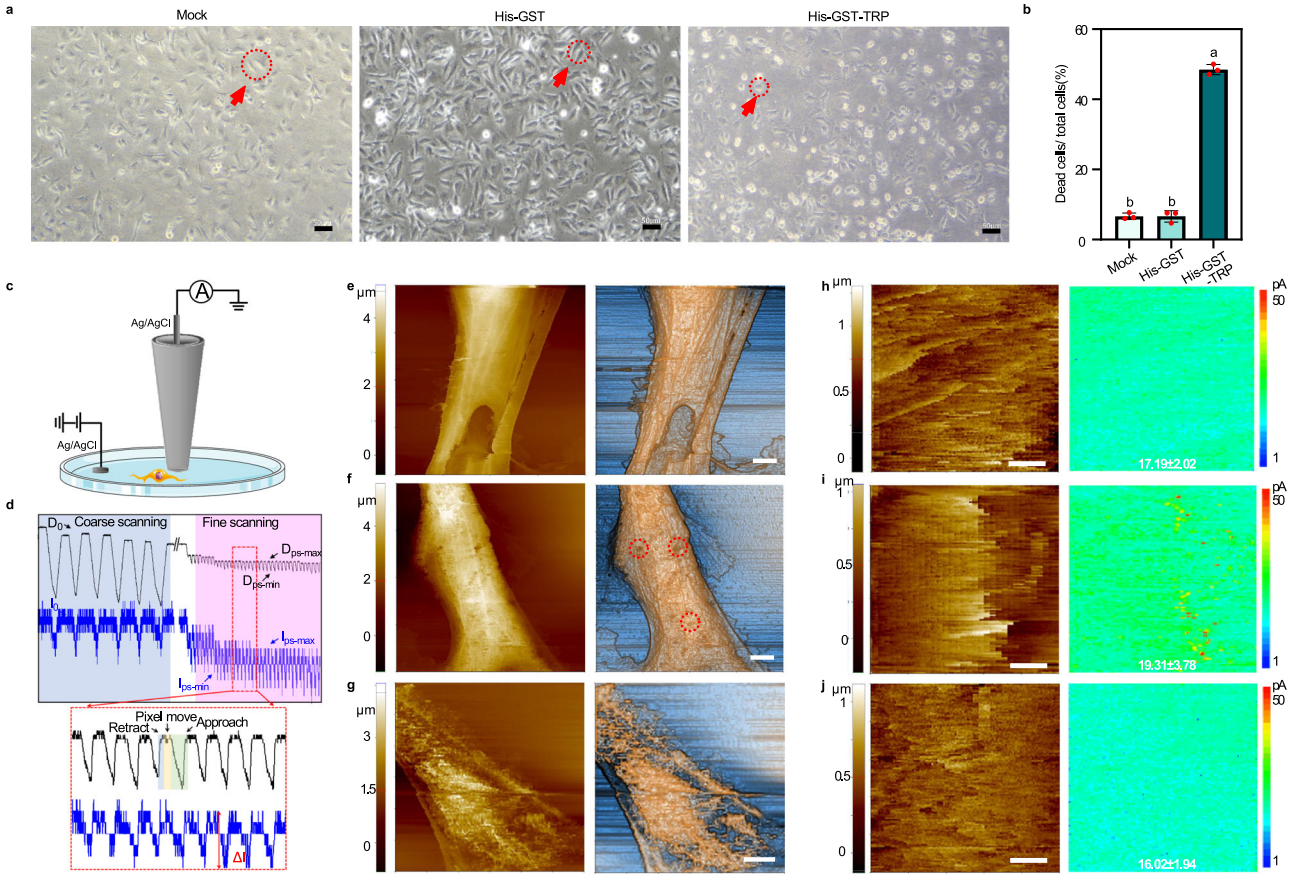

Fig. 4 | VdTRP damages cell membrane and causes cell death in mammalian cells. a Observation of rat cardiomyocyte cell morphology under light microscope. VdTRP treatment resulted in cell shape changes for rat cardiomyocytes, from normal growing wedge-shaped to round shape indicating dead cells, as shown by red arrow and red dash circles in respective panels. 50 μg/mL His-GST-TRP was used to treat cells for 2 min. **b** Cell death rate of rat cardiomyocytes in **a**. Data are shown as mean ± s.d. (n = 3 biologically independent experiments), different letters denote significant differences (p < 0.05) by one-way ANOVA with Duncan's multiple range tests. **c** Schematic diagram illustrating the device used to measure cell topography and surface charge by ΔI-SICM using a glass nanopipette as scanning probe. **d** Time traces of nanopipette movement and record of ionic current changes. An initial coarse scanning was performed followed by a fine scanning. The surface charge map was constructed using ΔI-SICM method. **e**–**g** Representative images of cell surface topography detected by ΔI-SICM. 2D and enhanced color topography images were shown in the left and right panels, respectively. The surface of normal-growing rat cardiomyocytes appears relatively smooth with a clear texture (**e**); cell membrane of rat cardiomyocytes treated with VdTRP protein shows signs of damage, with pores in their cell membranes, as indicated by red dash circles (**f**); some cells show severe membrane damage especially under longer incubation with VdTRP protein (**g**). In **e**–**g**, bars = 5 μm. **h**–**j** Representative images of cell topography (left panels) and surface charge at the corresponding positions (right panels). **h** Normal growing cells, no position with high ionic current were detected, and cell surface has an average ionic current value of 17.19 ± 2.02 pA (picoampere) in analyzed region; **i** cells exhibit initial cell damage after treatment with VdTRP protein; red and yellow points represent positions on cell membrane that show high ionic current. Cell has an increased average ionic current value of 19.31 ± 3.78 pA. **j** Cells displaying severe membrane damage have decreased average current value of 16.02 ± 1.94 pA, with many positions having very low ionic current as indicated by blue points. In **h**–**j**, bars = 1 μm. Source data are provided as a Source Data file.

The proline-rich motif in VdTRP is widely present in ascomycete fungi

Interestingly, when using IPGGCNPAHPGSCP motif as the query to do the Blast, we found that the motif is widely spread in effectors of diverse pathogenic fungi, such as in Verticillium, Fusarium, Botrytis, and Sclerotinia, and duplication of the motif frequently occurred in these effectors (Supplementary Fig. 5 and Supplementary Data 1). Phylogenetic analysis reveals that these fungi with the effectors belong to ascomycete phylum (Supplementary Fig. 6a, b). We selected several effectors with the repeat motif from different pathogenic fungi and tested their toxicity to plant cells. We observed that one effector from *Botrytis cinerea* (XP_001561412) caused severe cell death in *N. benthamiana*, while other effectors tested only caused weak cell death. Sequence analysis reveals that the effector from *B. cinerea* possesses a GPI membrane anchor sequence, while other effectors do not have any membrane targeting signal, which may explain why the *B. cinerea* effector but not others cause strong cell death (Supplementary Fig. 6c–e). Together, our data suggest that identified repeat motif exerts a specific virulence function on plasma membrane and is conserved across a number of fungal species.

VdTRP interacts with cotton CTL1

To identify the potential host targets of VdTRP, we conducted a yeast two-hybrid (Y2H) to screen VdTRP interaction proteins in a cDNA library constructed from *V. dahliae*-infected *Gossypium barbadense* acc. H7124 plant roots. This assay identified a candidate interacting protein which shared high homology with Arabidopsis chitinase-like1 protein AtCTL1[29], thus we designated the candidate protein CTL1 in this study. There are two copies of CTL1 in tetraploid *G. barbadense* acc. H7124 and *G. hirsutum* acc. TM-1 genome, with each one in A and D subgenome, respectively. Homoeologous CTL1s in A and D subgenome have 98.75% sequence identity, indicating that CTL1 is highly conserved in cotton (Supplementary Table 2). To validate the interaction in plant cells, we performed bimolecular fluorescence complementation (BIFC) and luciferase (Luc) complementation assays in *N. benthamiana*. BIFC assay

https://doi.org/10.1038/s41467-024-54470-0

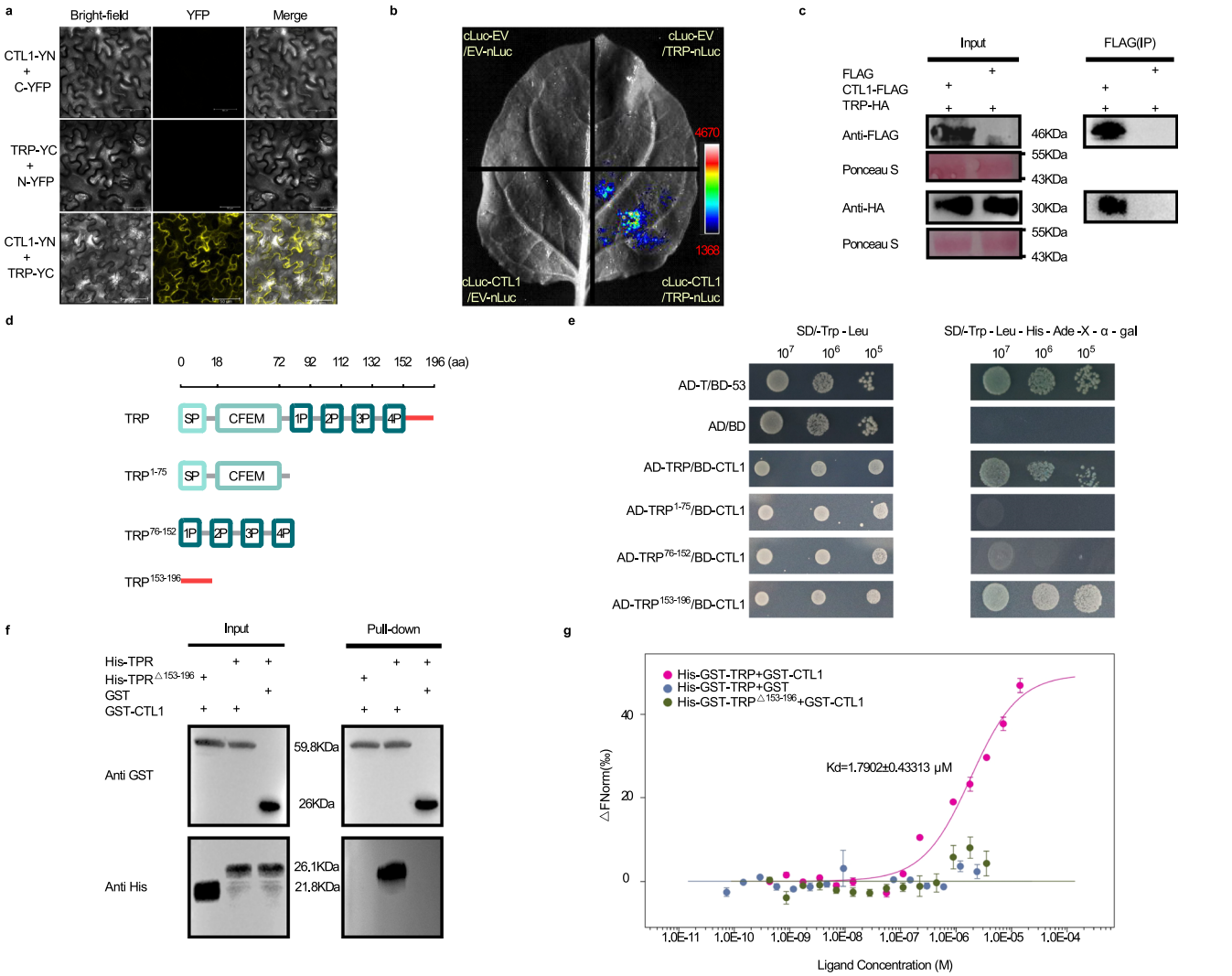

Fig. 5 | VdTRP interacts with a cotton chitinase-like 1 (CTL1) protein. **a** Confirmation of VdTRP interaction with CTL1 in plant cells by BiFC assay. Co-expression of CTL1-YN/TRP-YC in *N. benthamiana* cells could generate YFP signals, while negative controls CTL1-YN/YC, and YN/TRP-YC could not produce YFP signals. Scale bars: 50 μm. **b** VdTRP / CTL1 interaction was validated by luciferase complementation assays. Only co-expression of cLuc-CTL1/ TRP-nLuc produced signals, but negative controls cLuc-EV/EV-nLuc, cLuc-EV/TRP-nLuc, cLuc-CTL1/EV-nLuc could not produce signals. **c** Confirmation of VdTRP/CTL1 interaction by Co-IP assay. TRP-HA and CTL1-FLAG were co-expressed in *N. benthamiana*. Extracted proteins were subjected to Co-IP using FLAG-trap beads and western blotting with anti-HA and anti-FLAG, respectively. **d** Constructs for identification of the domain in TRP required for interaction with CTL1. Three truncated versions of VdTRP, TRP^{1-75}, TRP^{76-152}, and $TRP^{153-196}$ as well as full-length of TRP were used to test the interaction with CTL1 by yeast-two-hybrid. **e** The C-terminal $TRP^{153-196}$ interacts with CTL1 in Y2H. Double dropout (SD/-Trp/-Leu) was used as nonselective medium, while quadruple dropout (SD/−Trp/−Leu/−Ade/−His/X-a-gal) as selective media, positive interactions can grow and turn blue. Interactions of BD-Lam/AD-RecT and BD-53/AD-RecT were used as the negative and positive controls, respectively. **f** CTL1 can interact with full-length TRP but not the C-terminus deletion version $TRP^{\triangle 153-196}$ by pull-down assay. GST-CTL1 fusion protein was used as bait, and His-TRP fusion protein was used as prey. Anti-His antibody was used to detect prey proteins. GST/His-TRP were used as negative controls. **g** Microscale thermophoresis (MST) analyses show high binding affinities of TRP with CTL1, but $TRP^{\triangle 153-196}$ in which the C-terminus was deleted cannot bind CTL1. Binding of GST with TRP was used as negative control. Kd, dissociation constant. Data are shown as mean ± s.d. ($n = 3$ biologically independent experiments). YFP yellow fluorescent protein. VdTRP shortens as TRP. The experiment was independently repeated three times with similar results (**a**–**c**, **e**–**g**). Source data are provided as a Source Data file.

revealed that VdTRP/CTL1 complex localized on the peripheral region of plant cells, with some exhibited punctate distribution (Fig. 5a). Luc complementation assay showed that luciferase signals could only be clearly monitored at the site of infiltration co-expressing VdTRP-nLuc/cLuc-CTL1, whereas no signals could be detected in negative controls (Fig. 5b). Co-IP assay also confirmed the VdTRP/CTL1 interaction (Fig. 5c). To determine which domain of VdTRP is involved in interaction with CTL1, three domains of VdTRP were separately used to test the interaction with CTL1 by Y2H (Fig. 5d). The results indicate that it is the C-terminal domain other than the CFEM and the repeat domain that mediates the interaction with CTL1 (Fig. 5e). In vitro pull-down assay also confirms the VdTRP interaction with CTL1 (Fig. 5f).

We then used microscale thermophoresis (MST) assay to determine the Kd (dissociation constant) value between VdTRP and CTL1 interaction (Fig. 5g). The results showed that only His-GST-TRP/GST-CTL1 interaction could generate a small Kd value (Kd = 1.7902 μM), while His-GST-$TRP^{\Delta 153-196}$/GST-CTL1 interaction and the control His-GST-TRP/GST interaction could not generate Kd value. These assays demonstrate that the VdTRP strongly binds CTL1, but the C-terminal deletion version of VdTRP abolishes this binding.

https://doi.org/10.1038/s41467-024-54470-0

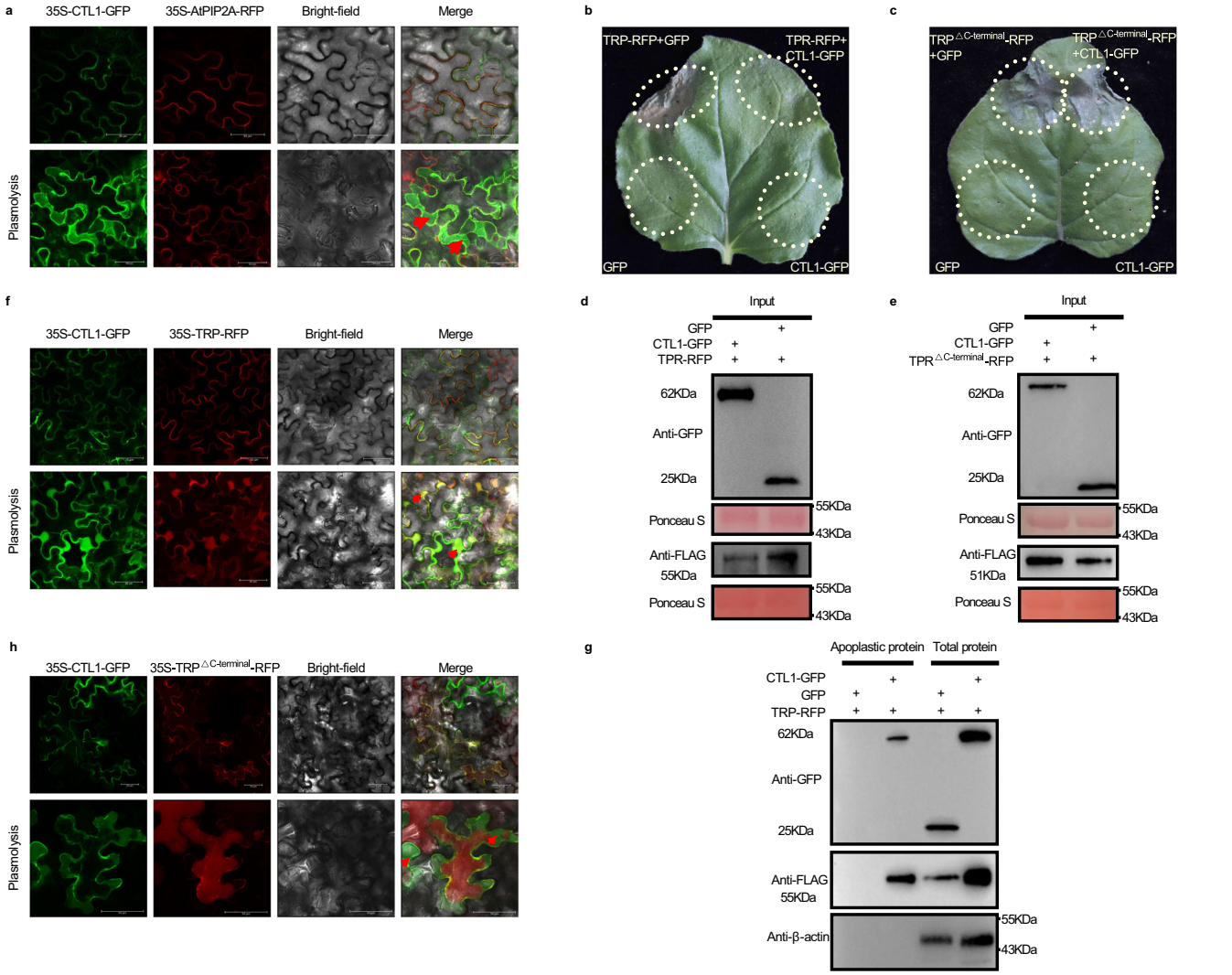

Fig. 6 | Co-expression CTL1 and VdTRP holds VdTRP in the apoplast and eliminates cell toxicity of VdTRP. a CTL1 is a secreted protein and localized in the apoplast. Plasmolysis show CTL1 is an apoplast-localized protein. Scale bars: 50 μm. **b** Co-expression CTL1-GFP and TRP-3×FLAG-RFP eliminates cell toxicity of TRP. GFP and CTL1-GFP were used as controls. **c** Co-expression of CTL1 with TRP$^{\triangle C\text{-terminal}}$−3×FLAG-RFP could not block cell toxicity, indicating that abolishment of CTL1/TRP interaction are unable to inhibit effector virulence. GFP and CTL1-GFP were used as controls. **d**, **e** Protein expression in **b** and **c** was confirmed by western blot using anti-GFP and anti-FLAG antibody, respectively. **f** CTL1-GFP and TRP-3×FLAG-RFP are colocalized in the apoplast. **g** CTL1 holds VdTRP in the apoplast was confirmed by western blot using apoplastic protein preparations. anti-GFP and anti-FLAG were respectively used to detect the presence of CTL1 and TRP in the apoplast. TRP-3×FLAG-RFP /GFP co-expression was used as negative controls. **h** TRP$^{\triangle C\text{-terminal}}$−3×FLAG-RFP localized in cytoplasm even in presence of CTL1-GFP, indicating that abolishment of TRP/CTL1 interaction, CTL1 could not hold TRP in the apoplast. In **a**, **f** and **h**, red arrows represent the apoplastic region of the cell. Scale bars: 50 μm. GFP green fluorescent protein, RFP red fluorescent protein. VdTRP shortens as TRP. The experiment was independently repeated three times with similar results (**a**, **f**, **g**). Source data are provided as a Source Data file.

CTL1 is an apoplastic protein which effectively reduce VdTRP toxicity by redirecting VdTRP from plasma membrane to apoplast

To explore the possible role of VdTRP association with CTL1 in the outcome of cotton- *V. dahliae* interactions, we first investigated the subcellular localization of CTL1 in plant cells. Similar to the Arabidopsis CTL1 ortholog[29], cotton CTL1 fused with GFP also localizes in the apoplast (Fig. 6a). We then co-expressed TRP-RFP and CTL1-GFP in *N. benthamiana* leaves and monitored the cell death phenotype. We observed that co-expressing TRP-RFP/CTL1-GFP significantly reduced the cell death compared with co-expressing TRP-RFP/GFP. In addition, transient expressing CTL1-GFP or GFP alone could not produce detectable cell death (Fig. 6b, Supplementary Fig. 7a). These results indicate that CTL1 may block the virulence of VdTRP. Interestingly, cell death clearly appeared when TRP$^{\triangle C\text{-terminal}}$-RFP (C-terminal deletion version of VdTRP) and CTL1-GFP were co-expressed, implying that abolishing VdTRP/CTL1 interaction recovered VdTRP virulence even in presence of excess CTL1 proteins (Fig. 6c, Supplementary Fig. 7b). The protein expressions of all constructs in planta were confirmed by western blot (Fig. 6d, e).

Protein localization is often connected to its functions. For examples, some bacterial toxins target on eukaryotic cell membranes and form pores in membrane, which causes cell leakage and subsequent cell death[30]. Similarly, in fungi, NLP protein toxins also target plasma membrane and forms transient pores leading to membrane leakage and cell death[31]. Since VdTRP exert its virulence function on plasma membranes and CTL1 can block VdTRP virulence. We monitored whether VdTRP/CTL1 association could change the subcellular localization of VdTRP and disable its virulence. As expected, we observed that VdTPR/CLT1 complexes largely distributed in the apoplast, demonstrating that VdTRP/CTL1 association indeed changed VdTRP localization (Fig. 6f). In addition, we were able to clearly detect

the presence of VdTRP in apoplastic protein preparations from *N. benthamiana* leaves co-expression VdTPR/CLT1. However, when TRP-RFP and GFP were co-expressed, VdTRP could not be detected in apoplastic protein preparations (Fig. 6g). These results demonstrated that VdTRP/CTL1 association indeed changed VdTRP localization, thus might abolish VdTRP virulence upon plasma membrane. Interestingly, $TRP^{\triangle C\text{-terminal}}$-RFP localized to plasma membrane and CTL1-GFP localized in apoplast when $TRP^{\triangle C\text{-terminal}}$-RFP / CTL1-GFP were co-expressed (Fig. 6h). This result suggests that C-terminal deletion in VdTRP abolishes VdTRP/CTL1 association and leads to inability of CTL1 to redirect $TRP^{\triangle C\text{-terminal}}$-RFP in the apoplast, thus $TRP^{\triangle C\text{-terminal}}$-RFP targets plasma membrane and causes cell death even in presence of excess CTL1. Together, our data support the notion that VdTRP exerts its toxic function on plasma membrane and once VdTRP membrane targeting is blocked by CTL1, it will lose its toxicity to plant cells.

CTL1 has no chitinase enzyme activity while contributes to wilt resistance

Sequence analysis show that CTL1 consists of 325 amino acids with a predicted N-terminal signal peptide and the GH19 domain in the central region (Supplementary Fig. 8a). Similar to other chitinase-like proteins in other plant species such as Arabidopsis and rice, cotton CTL1 is also devoid of the chitinase activity motif H-E-T-T[32], thus CTL1 should have no chitinase enzyme activity (Supplementary Fig. 8b). To confirm this, we expressed CTL1 as a glutathione-S-transferase (GST) fusion in *E. coli*, and the purified protein was used to perform in vitro antifungal assays. The results revealed that GST-CTL1 fusion was unable to inhibit *V. dahliae* in vitro (Supplementary Fig 8c–e), demonstrating that CTL1 has no antifungal activity. To test whether CTL1 has in planta enzyme activity, we transiently expressed CTL1-GFP fusion in *N. benthamiana* leaves, and measured the enzyme activity (Supplementary Fig. 8f). We were still unable to detect any chitinase activities of the fusion protein (Supplementary Fig. 8g). Thus, cotton CTL1 is indeed not a chitinase but a chitinase-like protein.

Since *CTL1* was highly induced upon *V. dahliae* infection in the resistant accession H7124 than in susceptible accession TM-1 (Supplementary Fig. 8h). We investigated the role of *CTL1* in cotton defense against *V. dahliae* attack. We utilized the virus induced gene silencing (VIGS) technique to silence *CTL1* in H7124 (Supplementary Fig. 8i). The *CTL1*-silenced cotton seedlings grown to the second true leaf stage were root-inoculated with *V. dahliae* spore suspensions, and disease symptoms were monitored from 11 to 35 days post inoculation. The results showed that *CTL1*-silencing compromised the resistance of H7124 upon *V. dahliae* infection (Supplementary Fig. 8j), as revealed by the increased percentage of wilted leaves (Supplementary Fig. 8k) and the fungal biomass in roots (Supplementary Fig. 8l). Our data demonstrate that *CTL1* contributes to cotton resistance upon *V. dahliae* attack.

CTL1 is essential for cotton growth and development

To further investigate the roles of *CTL1* in cotton growth and development, we generated stable *RNAi-CTL1* transgenic cotton plants. During the genetic transformation experiments, we observed that most of the transgenic lines were died in early stages of tissue culture. Despite of this effect, we were able to obtain five *RNAi-CTL1* cotton lines (Supplementary Fig. 9a). However, these lines exhibited severe stunted growth and failed to produce bolls and seeds (Fig. 7a). In addition, *RNAi-CTL1* plants displayed serious defects in lateral root growth (Fig. 7b, c). The stem cross-section observations showed that *RNAi-CTL1* plants had loosely packed and less vessel cells, as well as thinner xylem, compared with the controls (Supplementary Fig. 9b, c). Since loss of function of CTL1 in Arabidopsis affects cellulose biosynthesis and the function of CTL1 was proposed to be conserved across plant species[29], we therefore checked the expression of genes encoding cellulose synthase in *RNAi-CTL1* plants. It was found that cellulose synthase genes *GhCESA4*, *GhCESA7* and *GhCESA8* were rarely expressed in *RNAi-CTL1* plants, implying that CTL1 is involved in secondary wall formation in cotton (Supplementary Fig. 9d).

Since *RNAi-CTL1* plants are unable to produce progeny, we then turn to assess the role of *CTL1* in cotton growth and development using VIGS technique. Similarly, *CTL1* silencing also resulted in a defect in lateral root development, but not displayed such serious phenotypes as in *RNAi-CTL1* transgenic plants (Fig. 7d, e). We measured the total root length, root surface area, mean root diameter and the root tip numbers in TRV:*CTL1* and the TRV:00 cotton plants. It was shown that all these parameters in TRV:*CTL1* plants were significantly decreased compared with TRV:00 plants (Fig. 7f–i). Remarkably, similar to the maize *brittle stalk4* mutant, TRV:*CTL1* plants also displayed a brittle stalk phenotype (Fig. 7l and Supplementary Fig. 10c). Furthermore, TRV:*CTL1* plants grew much slower and displayed a stunted growth phenotype (Supplementary Fig. 10d, e). Measurement the content of sucrose, glucose, fructose and cellulose in stems of TRV:*CTL1* plants demonstrated that these components were significantly decreased compared with TRV:00 plants (Fig. 7m–p). The stem cross section observations with Safranine O-Fast Green Staining showed that the thickness of xylems in stems of TRV:*CTL1* plants became thinner, xylem vessels were looser, and the number of vessels was less than that in TRV:00 plants (Fig. 7q, r). These experiments demonstrate that *CTL1* silencing in cotton seriously affects the development of cell walls, especially the secondary wall formation.

Although *CTL1* disruption in cotton shares some common phenotypes with the CTL1 mutants in Arabidopsis, rice and maize[33,34], a striking different feature is that *CTL1* disruption in cotton results in serious dwarf stature and sterility. To investigate the underlying molecular mechanism, we performed the global gene expression profiles in stems of TRV:*CTL1* and TRV:00 plants by RNA-seq analysis. In total, 3632 differentially expressed genes (DEGs) ($q < 0.05$ and a fold change >1) were detected, including 1661 up-regulated genes and 1971 down-regulated genes in TRV:*CTL1* relative to TRV:00 plants (Supplementary Fig. 11a and Supplementary Data 2). GO enrichment analysis showed that transcriptional regulation and cell wall biogenesis ranked the most predominant pathways in down-regulated genes (Supplementary Fig. 11b). while the translation and photosynthesis were the major pathways in up-regulated genes (Supplementary Fig. 11c). For instances, *CTL1* silencing resulted in down-regulation of more than 200 transcription factors, including *GhNST1*, *GhSND1*, *GhSND2*, *GhMYB103*, *GhMYB4*, and *GhMYB61*, these genes were previously reported to be associated with secondary cell wall metabolism[35–38] (Supplementary Fig. 11d). The transcripts of genes involved in glycometabolism[36], cellulose synthase, receptor proteins, and protein phosphatase related genes were decreased in *CTL1*-silenced plants (Supplementary Fig. 11e–h). Remarkably, *CTL1* silencing causes up-regulation of 227 ribosome proteins encoding genes and 64 photosynthesis-related genes (Supplementary Fig. 11i), which might reflect an attempt to keep protein synthesis and photosynthesis at optimal levels when cell growth encountered serious retardation in TRV:*CTL1* plants. Together, our data reveal that CTL1 disruption in cotton seems to make cells in a serious stress state so as to result in a tremendous reprograming of gene expressions, which might explain why CTL1 is essential in cotton growth and development.

CTL1 overexpression enhances wilt resistance of cotton by elevating the basal level of sugar and salicylic acid

We have shown that *CTL1* silencing by VIGS compromises cotton resistance against *V. dahliae* infection. We then investigate whether CTL1 overexpression can improve cotton resistance to *V. dahliae* attack. We generated stable transgenic cotton plants overexpressing *CTL1* driven by 35S promoter. A total of seven *CTL1*-overexpressing transgenic lines were obtained (Supplementary Fig. 12a, b). Four lines with higher *CTL1* expression level were selected to assess their

https://doi.org/10.1038/s41467-024-54470-0

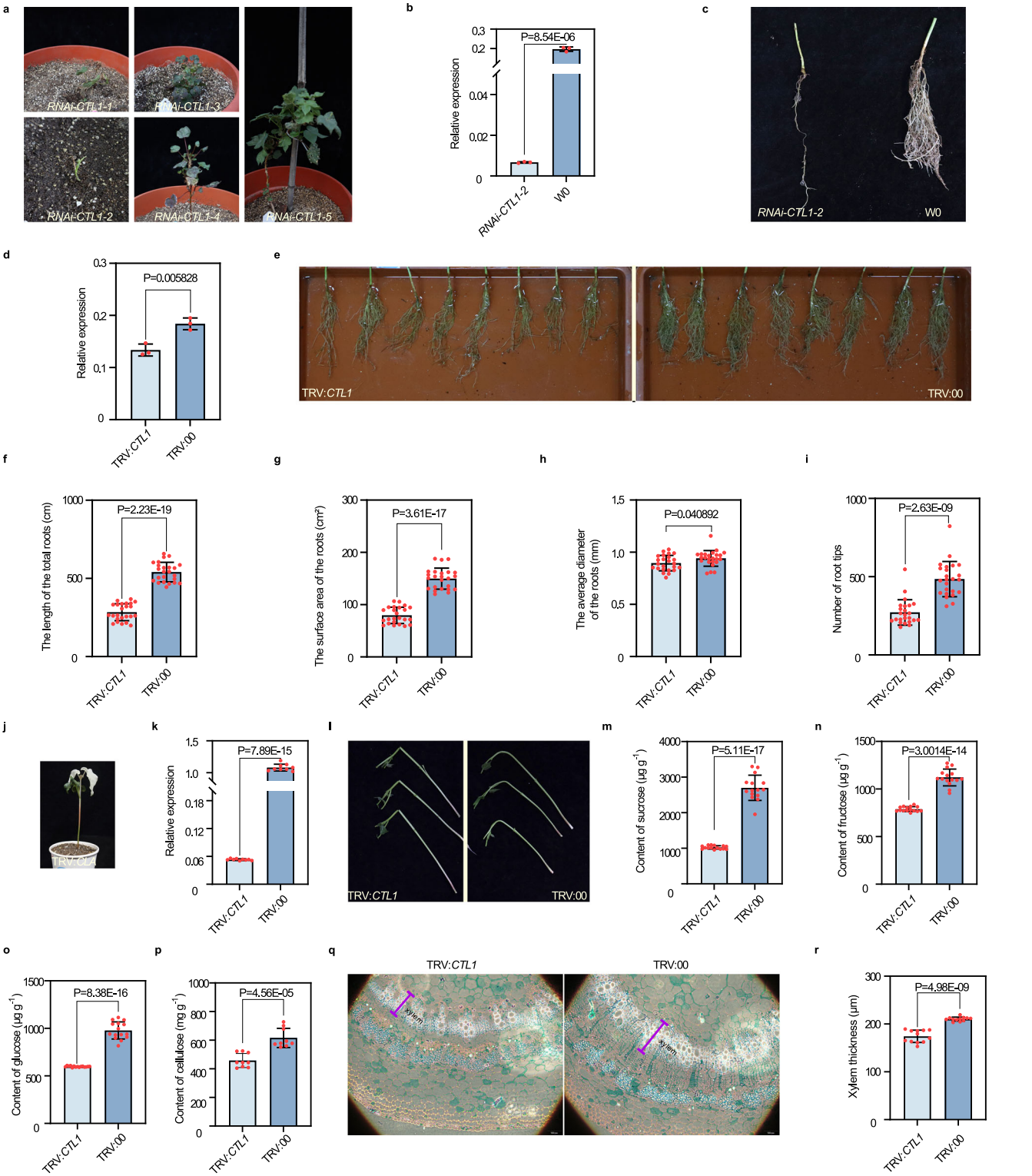

resistance. Infection assays showed that all these lines exhibited substantially enhanced resistance to *V. dahliae* (Supplementary Fig. 12c, d). Two lines, OE138 and OE172, exhibiting the highest *CTL1* expression level, were selected to conduct the following assays. As shown in Fig. 8, OE138 and OE172 displayed substantially decreased percentage of wilted leaves, fewer fungal accumulation in vascular and less fungal biomass in roots (Fig. 8a–d). Fungi recovery assay showed that less fungi were recovered from the stems of OE138 and OE172 lines infected with *V. dahliae* compared with the non-transgenic line (Fig. 8e). Furthermore, we transiently expressed VdTRP in cotton cotyledons of both transgenic and non-transgenic lines by agroinfiltration. It was shown that less cell death was observed and decreased electrolyte leakage was detected in cotton cotyledons of OE138 and OE172 lines than that in non-transgenic line (Fig. 8f, g).

To investigate the molecular mechanisms of CTL1 in promoting wilt resistance in cotton, we studied the global gene expression profiles in OE138 and OE172 compared with non-transgenic line by RNA-seq technique. Cotton seedling at the second true leaf stage were root inoculated with *V. dahliae* suspension spores. Root samples at 72 h post inoculation and the mock treatments were collected. The RNAs of

Fig. 7 | CTL1 is essential for cotton growth and development. a T_0 plants of transgenic *RNAi-CTL1* cotton died in the seedling stage, or failed to produce boll and seeds. **b** Relative expression of *CTL1* in *RNAi-CTL1-2* cotton roots showing that *CTL1* was successfully silenced. Data are shown as mean ± s.d. (n = 3 biologically independent experiments). **c** Root development of *RNAi-CTL1-2* was seriously affected. **d** Verification of *CTL1* silencing by RT-qPCR in TRV:00 and TRV:*CTL1* plant roots. Data are shown as mean ± s.d. (n = 3 biologically independent experiments). **e** *CTL1*-silenced plants exhibit retarded root growth and development. Compared with TRV:00, the total roots length (**f**), the roots surface area (**g**), the mean roots diameter (**h**), and the number of root tips (**i**) of the *CTL1*-silenced plants were significantly decreased. Data are shown in **f**–**i** as mean ± s.d. (n = 24 biologically independent experiments). **j** TRV:*CLA* was used as a positive control. **k** Verification of *CTL1* silencing by RT-qPCR in TRV:00 and TRV:*CTL1* plant leaves. Data are shown as mean ± s.d. (n = 9 biologically independent experiments). **l** TRV:*CTL1* plants showed brittle stalks phenotype compared with TRV:00. Compared with TRV:00 plants, the content of sucrose (**m**), glucose (**n**), fructose (**o**) and cellulose (**p**) in stems of the *CTL1*-silencd plants were significantly decreased. Data are shown in **m**–**o** as mean ± s.d. (n = 15 biologically independent experiments). Data are shown in **p** as mean ± s.d. (n = 9 biologically independent experiments). **q** Xylem thickness in TRV:*CTL1* stems were significantly reduced. The transverse representative stems section stained with Safranine O-Fast Green Staining were observed. The purple lines indicate xylem thickness. Scale bars: 100 μm. **r** Statistical analysis of the xylem thickness in **q**. Data are shown as mean ± s.d. (n = 12 biologically independent experiments). All statistical analyses were performed by the two-tailed Student's t test. *G. hirsutum* acc. W0 was used as transgenic receptor. *G. hirsutum* acc. TM-1 was used for VIGS analysis. Source data are provided as a Source Data file.

these samples were extracted and subject to RNA-seq assays. Relative to the control W0, 1589 and 1710 DEGs were detected in line OE138, under mock treatment and pathogen stress, respectively. Similarly, 2357 and 2490 DEGs were detected in line OE172 under same conditions. Among these, 586 DEGs are shared by OE138 and OE172 (Fig. 9a, b and Supplementary Data 3).

GO analysis for these 586 DEGs revealed that the defense responses and regulation of SA metabolic process were two major pathways enriched (Fig. 9c). RT-qPCR revealed that *CTL1* overexpression led to up-regulation of chorismite synthase encoding gene *GhCS1* and SA biosynthesis-related gene *GhICS2*, and down-regulation of *GhPNP-A*, which is involved in SA repression[39,40]. Furthermore, transcripts of *GhPR1*, *GhPR5-like* and *GhPR11* (pathogenesis-related genes) were significantly increased (Fig. 9d). To validate these results, we measured the SA content in *CTL1* transgenic and non-transgenic lines. It was shown that SA levels in OE138 and OE172 were significantly higher than that in non-transgenic control W0 (Fig. 9e). We also observed that the transcripts of a large number of disease resistance genes and leucine-rich repeat receptors were enriched (Supplementary Fig. 13a, b). Two receptor kinases genes *GhWAK2* and *GhPR5K*, which was previously reported to respond to *V. dahliae* infection[41,42], were also detected (Supplementary Fig. 13c).

It has been reported that *CTL1* overexpression in maize leads to increased cellulose biosynthesis and enhanced mechanical stalk strength[33], we thus hypothesize that *CTL1* overexpression in cotton might have similar effects. Intriguingly, we could not detect the increases in cellulose content in OE138 and OE172 stems (Supplementary Fig. 14). Then we ask whether *CTL1* overexpression might result in changes in sugar content. We thus measured the contents of 26 kinds of sugars and sugar alcohols in roots of OE138 and OE172 lines and the control W0 (Supplementary Data 4). We were able to detect changes of fourteen sugars and sugar alcohols (Fig. 9f). Interestingly, contents of sucrose, fructose, glucose, and ribose in roots of OE138 and OE172 were significantly increased (Fig. 9g). Whereas, no obvious changes in expression of genes relating to sucrose synthesis could be detected (Supplementary Fig. 13d). We hypothesize that *CTL1* overexpression might increase the photosynthesis in cotton leaves, and the sugar increase in root tissue may derive from the source to sink transport, excess sugar might induce sugar-triggered immune responses. To evaluate the potential application of *CTL1* in breeding cotton with high wilt resistance, we assessed the field performance of OE138 and OE172 lines in a small scale. Preliminary investigation showed that there were no obvious negative impacts of *CTL1* overexpression on cotton growth and development. In addition, fiber quality traits and yield components were substantially unchanged compared with non-transgenic line, making this gene with potential application in breeding (Supplementary Fig. 15).

Discussion

V. dahliae causes destructive vascular wilts in a wide range of economically important crops, including cotton, posing a big threat to agriculture[43]. No germplasm of upland cotton, accounting for more than 90% of the world's total cotton output, is immune to Verticillium wilt[44]. Studying how the fungal pathogen subvert host defenses may be an alternative way to find strategies to combat the disease caused by this pathogen. In the present study, we identified an effector VdTRP in a cotton pathogenic *V. dahliae* strain V991, which was demonstrated to constitute a member of protein toxins. VdTRP contains a non-canonical CFEM domain and a tandem repeat domain rich in proline. CFEM mediates the membrane targeting and the repeat domain might play a role in membrane toxicity causing membrane leakage and subsequent cytolysis. Both the two domains are required for full virulence of VdTRP. Furthermore, by VdTRP effector-assisted screening, we identified its host target, which is an apoplastic protein whose ortholog in Arabidopsis has been proved to regulate cellulose biosynthesis and mediates interactions between cellulose microfibrils and hemicelluloses. We provide evidence that excess CTL1 protein could change the localization of VdTRP or block VdTRP from entering into plant cells thus reducing its toxicity to plant cells. Our data demonstrate that the effector-assisted identification of host proteins will accelerate the discovery of candidate genes used for genetic manipulation and improve crop resistance.

Both CFEM and the repeat domain is critical for VdTRP cell toxicity

Although the CFEM domain in VdTRP contains six cysteine residues, which is different from the canonical CFEM that possesses eight conserved cysteine residues[45], protein structure analysis suggested that VdTRP did contain a N-terminal CFEM domain, perhaps that the structure of CFEM in VdTRP is similar to that of CFEM members. 3D structural modeling revealed CFEM domain in VdTRP could form three predicted α-helices, which might be required for VdTRP membrane targeting. CFEM mediating membrane targeting was experimentally confirmed by investigation subcellular localization of full VdTRP compared with VdTRP$^{\Delta CFEM}$ mutant in which CFEM was deleted. The VdTRP$^{\Delta CFEM}$ protein no longer uniquely target on plasma membrane but also localizes in cytoplasm and nucleus, and significantly reduces virulence to plant cells. Furthermore, lipid-protein interaction assays reveal that full-length VdTRP strongly binds an important surface lipid, phosphatidylserine (PS), which has been shown to regulate cell surface charge and protein localization[46], while CFEM deletion abolishes this binding property. This experiment uncovers the molecular mechanism of VdTRP membrane targeting through CFEM strong binding with PS. Interestingly, two CFEM effectors VdSCP76/77 in *V. dahliae* was also reported to target on plasma membrane, whereas, they were shown to function in suppressing cell death, an opposite function to VdTRP[47]. It is possible that VdSCP76/77 may play a role in biotrophic stage of infection but VdTRP functions in necrotrophic stage.

Although CFEM domain-containing effectors or repeat domain-containing effectors in filamentous fungal pathogens are well reported in recent years[48], effectors combining the two domains have not been found in literatures. The repeat domain plays diverse roles in the

https://doi.org/10.1038/s41467-024-54470-0

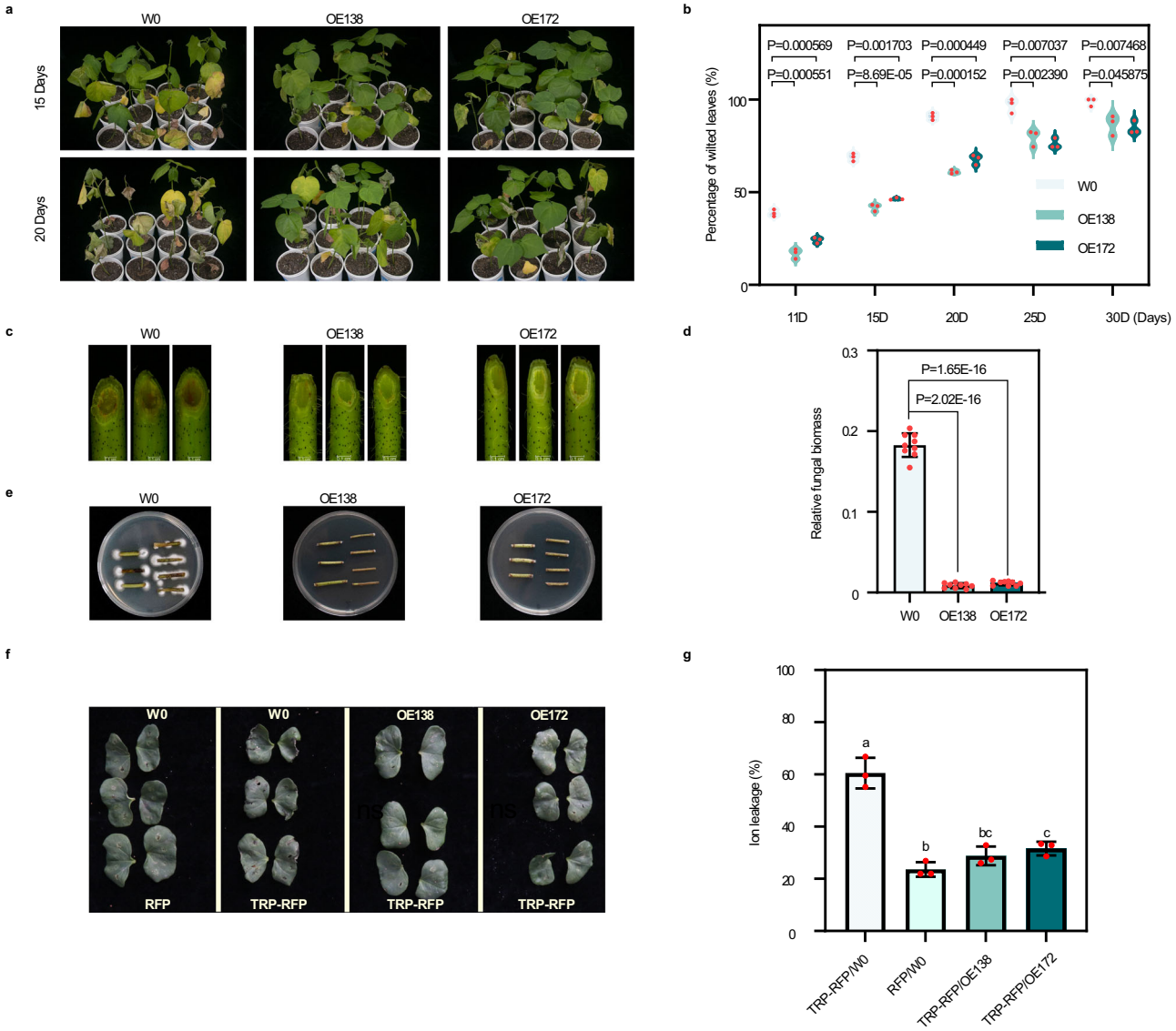

Fig. 8 | Overexpression of *CTL1* enhances Verticillium wilt resistance in cotton. **a** *CTL1* overexpression enhances wilt resistance in cotton. Phenotypes of the wild-type (W0) and the *CTL1*-overexpressing (OE) plants infected with *V. dahliae*. Photographs were taken at 15- and 20-days post *V. dahliae* inoculation. **b** Percentage of wilted cotton leaves inoculated with *V. dahliae*. The points represent three biological repeats ($n = 3$). Each biological repeat contains 10 seedlings. **c** Vascular discoloration in the W0 and the *CTL1*-overexpressing plants after inoculation with *V. dahliae*. **d** Quantification of fungal biomass in W0 and *CTL1*-overexpressing plant roots after 15 days post inoculation with *V. dahliae* by qPCR. Data are shown as mean ± s.d. ($n = 9$ biologically independent experiments). In **b** and **d**, all statistical analyses were performed by the two-tailed Student's *t* test. **e** Fungal recovery experiments. Plant stem sections of 15 days post inoculation were cut and placed on potato dextrose agar plates, and incubated at 25 °C. Photographs were taken at 4 days after culture. **f** Cotton cotyledons from the OE138 and OE172 lines produced less necrosis than non-transgenic line in response to transiently expressed VdTRP. Empty vector with RFP tag was used as negative control. The agroinfiltration technique was used to transiently express RFP and VdTRP in the cotyledon. **g** Degree of cell death in **f** was determined by ion leakage assay. Data are shown as mean ± s.d. ($n = 3$ biologically independent experiments), different letters denote significant differences ($p < 0.05$) by one-way ANOVA with Duncan's multiple range tests. VdTRP shortens as TRP. Source data are provided as a Source Data file.

biological function of repeat-containing effectors from plant-associated organisms, especially in the arm race between pathogen and their host. These roles can range from directing effector localization, mediating interaction with specific DNA, RNA or protein, and providing effector stability[49,50]. To our knowledge, the role in mediating membrane toxicity has not been reported. This function might be mediated by the specific proline-rich tandem repeat region. Because proline is a very unusual amino acid among the amino acid constituents of proteins, which possesses a unique conformation. It is supposed to be a disrupter of hydrogen bonding in both α-helices and β-sheets, which produces well-known helix-breaker and beta-sheet breaker effect. Uninterrupted polyproline tracts are more rigid than other sequence, and proline-rich motifs have conformational constraints that govern the structures of proteins that contain them. The rigidity of proline-rich motifs has important consequences for binding[51,52]. For instances, most membrane-enveloped viruses bud from infected cells by hijacking host ESCRT (the endosomal sorting complexes required for transport) machinery. To promote budding, ESCRTs are recruited to the budding sites by viral proteins that contains short proline-rich motifs known as late domains[53]. The human tumor-associated polymorphic epithelial mucin has a 20-residue proline-rich sequence repeated between 21 and 125 times[54]. It is heavily glycosylated and is thought to function by creating an extensive network of interlocking extended chains anchored to the membrane. In this study, by visualizing the dynamic topography and surface charge distribution mapping in rat cardiomyocyte cells upon VdTRP treatment, we demonstrate that VdTRP, which possesses four proline-rich repeat

https://doi.org/10.1038/s41467-024-54470-0

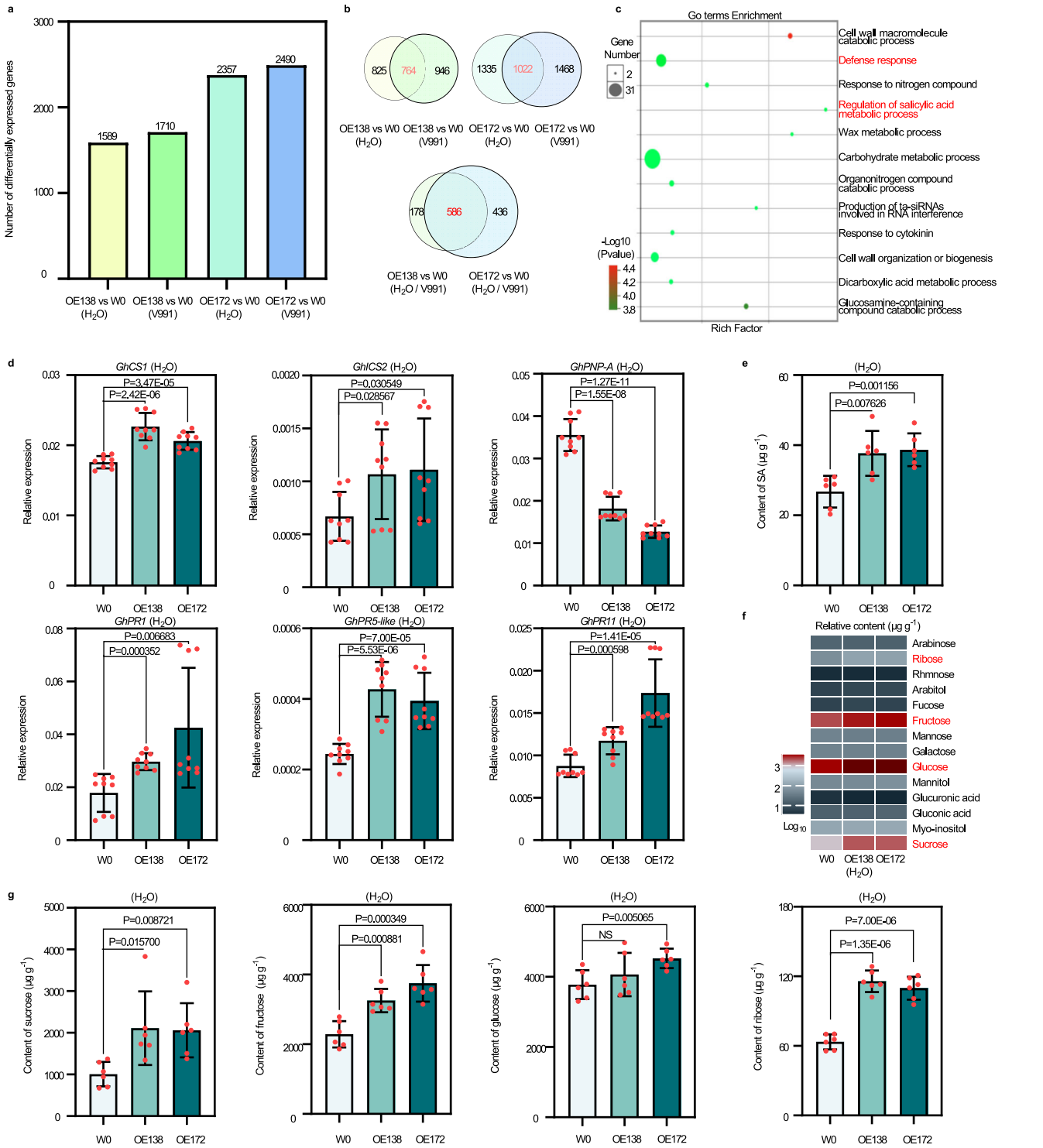

Fig. 9 | Overexpression of *CTL1* increases the basal SA level and sugars content. **a** Differentially expressed genes (DEGs) identified in *CTL1*-overexpressing lines compared to control W0 under water and pathogen inoculation analyzed by RNA-seq. **b** A total of 586 DEGs are common in *CTL1*-overexpressing lines compared with W0, under natural growth condition or inoculation with *V. dahliae*. **c** Pathway analysis for 586 DEGs in **b**, showing that pathways focus in defense response and regulation of SA metabolic process. The *p* value of 0.05 adjusted by false discovery rate. Rich factor indicates the percentage of enriched genes compared with background in corresponding gene ontology (GO) term. **d** Expression analysis of SA pathway related genes and PR genes in *CTL1*-overexpressing plants under water treatment. Data are shown as mean ± s.d. (n = 9 biologically independent experiments). **e** Determination of SA content in roots of *CTL1*-overexpressing lines and control W0, under water treatment. Data are shown as mean ± s.d. (n = 6 biologically independent experiments). **f** Heatmap of sugars and sugar alcohols content in roots of *CTL1*-overexpressing transgenic plants versus non-transgenic control by GC-MS. **g** Content of sucrose, fructose, glucose, and ribose in the roots of *CTL1*-overexpressing lines was significantly increased compared with the non-transgenic control line. Data are shown as mean ± s.d. (n = 6 biologically independent experiments). All statistical analyses were performed by the two-tailed Student's *t* test. NS no significance. Source data are provided as a Source Data file.

motifs, is also detrimental to mammalian cells, and show that VdTRP can generate pores on rat cardiomyocyte cell surface, which may induce rapid cell collapse and death. This investigation uncovers, at least in part, the mechanism of how VdTRP toxin functions on cell surface and induce rapid cell death. We hypothesize that similar actions should be used by VdTRP on plant cell surface. Natheless, it is still need to further clarify what VdTRP exactly does to plant cells although the SICM results provide a clue on how VdTRP works on mammalian lipid membranes.

IPGGCNPAHPGSCP motif are widely spread in effectors of diverse fungal pathogens

Blast analysis reveal that the 14-amino acid proline-rich motif is present in more than two hundred effectors of diverse fungi, specific in phylum of ascomycete. We observed that the number of the motif in each individual effector ranged from one copy to fifteen copies (Supplementary Data 1). For examples in genus Verticillium, effectors from *V. dahliae* strain usually have four copies of the repeat motif, while effectors from *V. alfafae* and *V. longisporum* strains have as many as eight copies. In Aspergillus, effectors from different isolates have two to ten copies. Interestingly, we identified 79 effectors containing the repeat motif in different isolates from Fusarium, and found that the motif had the mostly wide distribution in different isolates, while the duplication events were mostly occurred in effectors from Monilinia, with as many as 12-15 copies of the repeat motif in different effectors. These data suggest that the repeat motif has widely spread in effectors of diverse fungi during evolution, possibly by horizontal gene transfer from a common ancestor. However, to perform the virulence function on plasma membrane, the repeat motif/region should combine with a membrane targeting signal such as the CFEM domain or GPI membrane anchor sequence.

Excess CTL1 blocks VdTRP toxicity and induces plant immune response

By VdTRP-assisted screening, we identified its host target, the chitinase-like1(CTL1) in cotton. The CTL1 ortholog in Arabidopsis was previously shown to be an important component in cell walls, and played a role in cellulose biosynthesis and in establishing interactions between cellulose microfibrils and hemicellulose[30]. In maize, disruption CTL1 function displays a brittle stalk, dwarf stature, and semi-sterility of pollen[34]. In rice, mutation of CTL1 causes reduced cellulose content and mechanical strength but without obvious alterations in plant growth[33]. Our results show that disruption CTL1 function in cotton results in serious defects in cotton growth and development, suggesting CTL1 is an essential protein in cotton, whose functions might be diverged from the orthologs of monocot plant species such as rice. These data indicate that CTL1 orthologs constitute an important component of cell walls essential for plant morphogenesis. Thus, VdTRP targeting CTL1 may disrupt cell wall integrity and is a smart strategy for promoting fungal colonization. One can imagine that VdTRP performs dual functions: disrupt cell wall integrity by targeting CTL1 and kill cells by causing plasma membrane leakage.

Though VdTRP fulfils the above mentioned two functions on host plant cells, our data demonstrate that overexpressing the VdTRP target protein CTL1 can block the toxicity of VdTRP. Excess CTL1 proteins will associate with VdTRP effector proteins and hold VdTRP in the apoplast, in this case, VdTRP will be unable to enter plant cells and target on plasma membrane to disrupt integrity of cell membranes and induce rapid cell death. Meanwhile, excess CTL1 proteins can also meet the requirements of cell walls under pathogen attack. Furthermore, CTL1 overexpression increase the sugar level in roots, which might derive from source to sink transfer, and leads to sugar-triggered defense. Thus, CTL1 overexpression enhances wilt resistance of cotton.

We have described in a recent report that overexpression lysophospholipase, an essential protein of cotton, can overcome the toxic effects of VdNLP1, a well reported fungal protein toxin[22]. In the present study, we report that overexpressing a cell wall essential component CTL1 in cotton can counteract the fungal protein toxin VdTRP. Our discovery adds another example on how plants use an essential protein to combat fungal protein toxins produced by the hemi-biotrophic fungal pathogen *V. dahliae*. Furthermore, our study indicate that pathogen effector-assisted host gene cloning constitutes an alternative approach to rapidly identify potential genes that might be used for genetic manipulation to improve disease resistance of crops, which may accelerate breeding for crop disease resistance. In addition, our results reveal that genetic manipulation the expression of some essential genes maybe a potential strategy for plants/crops to combat toxin producing fungal pathogens, such as the hemibiotrophic fungal pathogen *V. dahliae*, which forms another layer of immune system except the PTI and ETI immune system.

Methods

Plant materials and culture conditions

Cotton accessions (*G. barbadense* acc. H7124, *G. hirsutum* acc. TM-1 and *G. hirsutum* acc. W0) and transgenic *CTL1* cotton lines with *G. hirsutum* acc. W0 as genetic transformation receptor were grown in the field with conventional agronomic practices at the cotton experimental bases of Nanjing Agricultural University in Anhui, China (118° E, 32° N) and Hainan, China (108° E, 18° N) for field investigation. The seedlings were grown in the controlled environment chamber under the following conditions: cotton (light 16 h (28 °C)/dark 8 h (25 °C)), *N. benthamiana* (light 16 h (26 °C)/dark 8 h (23 °C)), and Arabidopsis (light 16 h (23 °C)/dark 8 h (21 °C)), for laboratory analysis.

V. dahliae strain culture and inoculation treatments

The virulent strain of *V. dahliae* V991 was preserved in our laboratory. The V991 was cultured on potato dextrose agar (PDA) for 5 days and then transferred to liquid Czapek medium for another 5 days. After this, it was diluted with sterile water to a concentration of 1×10^6/mL conidial suspension and used to inoculate the cotton plants.

RNA extraction and RT-qPCR analysis

RNA was extracted using the FastPure Universal Plant Total RNA Isolation Kit (RC411, Vazyme Biotech Co., Ltd). Reverse transcription quantitative PCR (RT-qPCR) was performed using SYBR green real-time fluorescent quantitative enzyme.

Transcriptome sequencing and data analysis

Cotton seedlings was inoculated with *V. dahliae*. The total RNA of cotton root tissues with different time points inoculated and control was individually extracted to construct the RNA-seq library. Similarly, the RNA of *V. dahliae* V991 samples induced by cotton seedling roots at different time points was extracted to construct the RNA-seq library. Sequencing was performed using Illumina NovaSeq6000 platform. After the adapters were removed using Cutadapt.HTSeq program, the reads were mapped to the *G. hirsutum* acc. TM-1 (NAU_v2.1) genome (http://cotton.zju.edu.cn/download.html) and *V. dahliae* V991 genome (https://www.ncbi.nlm.nih.gov/bioproject/PRJNA453648) using a Hisat2 with the default settings, respectively, then calculated the quantity of matched reads, which was subsequently loaded into R statistical software for DEG analysis using DESeq2. By using FPKM analysis, gene expression data were standardized. Hierarchical clustering analysis and GO analysis were carried out using the Omicshare website (https://www.omicsshare.com/).

Bioinformatics analysis

The signal peptide was predicted in website (https://services.healthtech.dtu.dk/services/SignalP-5.0/)[55]. The 3D structural analysis of VdTRP was performed in SWISS-MODEL (https://swissmodel.expasy.org/)[56] and by AlphaFold (https://colab.research.google.

com/github/sokrypton/ColabFold/blob/main/AlphaFold2.ipynb)[57]. The protein domain was predicted in website (http://smart.embl-heidelberg.de/smart/set_mode.cgi?NORMAL=1)[58].

Plasmid construction and plant transformation

The open reading frame (ORF) sequence of *CTL1* in *G. barbadense* acc. H7124 was cloned and inserted into the *pBI121* vector with *Bam*HI and *Sac*I restriction enzyme sites to construct the *CTL1* overexpression vector. The *CTL1*-specific 300 bp forward sequence with *Bam*HI and *Xba*I restriction enzyme sites and reverse sequence with *Xho*I and *Eco*RI restriction enzyme sites were connected to the *pART27* vector to construct the *CTL1* interference expression vector. The *Agrobacterium tumefaciens*-mediated genetic transformation was performed following the method described previously[59].

Agrobacterium-mediated infiltration assays

The ORF sequence of *VdTRP*, and different truncated versions were constructed into *pCAMBIA1300-3×FLAG-RFP* vectors and transformed into *Agrobacterium GV3101*, respectively. *Agrobacterium tumefaciens* was re-suspended in MES buffer (10 mM $MgCl_2$, 10 mM morpholinoethanesulphonic acid, 100 µM acetosyringone [pH = 5.7]), and the necrotic phenotype was observed 3 days after *N. benthamiana* injection.

Trypan blue dyeing

The leaves sampled were fully submerged in the trypan blue working solution. The solution was heated and boiled for 10 min. Afterward, the samples were stayed overnight at 37 °C and finally removed the color to use the decolorizing solution for observation.

Generation of *VdTRP* knockout and complementation strains

To generate the *VdTRP* knockout mutants, about 1000 bp upstream and downstream sequences flanking *VdTRP* were amplified from the V991 genomic DNA. According to the previous methods in our laboratory[59], the fragments were inserted into the flanking regions of a hygromycin-resistance cassette (*HPH*) in *pDHt2* vector to generate *pDHt2-Up-HPH-Down*. The knockout mutant was obtained by *Agrobacterium transformation*. To complement *VdTRP* in the △*vdtrp* mutant, the 1000 bp promoter sequence of *VdTRP* and the full length of the gene were constructed into *pCOM* vector. The retrofit mutant was obtained by *Agrobacterium tumefaciens* method[58].

Disease assays

The roots of cotton seedlings at the second true leaf stage were inoculated with 30 mL *V. dahliae* conidial suspension (1×10^6 conidia/mL). *V. dahliae* disease symptoms were recorded starting 11 days after inoculation, and the percentage of wilted to healthy leaves were calculated accordingly.

Vascular discoloration assays

Fifteen days after inoculation with *V. dahliae*, an oblique splitting experiment was conducted on different cotton plants at the same location (1 cm above the cotyledon knot). The phenotype was observed and photographed under a stereoscope (DVM6a Lecia, Germany).

Fungal recovery experiments

The cotton seedlings were inoculated with *V. dahliae* V991 for 15 days, the plant stems were sliced, and sterilized with 70% alcohol, cultured on PDA for 3–5 days. The phenotype was observed and photographed.

Fungal biomass assays

Total DNA was extracted from cotton root tissues 15 days after inoculation with *V. dahliae*. Fungal biomass was determined by quantitative real-time PCR (qPCR) with the fungal-specific primer ITS-F based on the internal transcribed spacer of ribosomal DNA in combination with the *V. dahliae*-specific reverse primer STVe1-R. Cotton histone 3 (AF024716) was as an endogenous control[60].

Electrolyte leakage assay

Cell death induced by effectors was analyzed by measuring ion leakage from leaf discs as described by Wang et al.[61]. Six leaf discs (d = 0.8 mm) from agriculturally infiltrated leaves were collected and floated with shaking at 80 rpm in 4 mL of sterile water for 2 h. Ion leakage was quantified by analyzing the conductivity of water before and after sample boiling.

Preparation of Arabidopsis protoplast

Arabidopsis protoplasts were extracted as described in the protoplast kit (Plant Protoplast Preparation and Transformation kit plus, Realtimes, Beijing, China). Briefly, 0.1 g Arabidopsis leaves were cut into 0.5-1 mm strips. The leaf strips were added to 5 mL of enzymatic solution and incubated in the dark at room temperature for 3 hours. 5 mL of solution II was added to the enzymatic solution, mixed gently, and filtered through 70 µm nylon cell strainers to collect the filtrate. The filtrate was centrifuged at 100 × *g* for 2 min at room temperature, and the supernatant was removed as much as possible. The pellet was added to 5 mL of solution II, and the cells were resuspended and allowed to rest on ice for 30 min. The resuspension was centrifuged at 100 × *g* for 2 min at room temperature, the supernatant was removed as much as possible, and 1 mL of solution III was added to obtain a protoplast solution.

Toxicity of VdTRP and its various mutants on Arabidopsis protoplast

A total of 100 µL of purified His-GST-TRP and His-GST proteins (1 mg/mL) were respectively added to 100 µL of Arabidopsis protoplast solution. To continuously record cell changes under VdTRP stress, the mixture was immediately placed on a concave slide and video was recorded and lasted for 5 min under the microscope (BX51 Olympus, Japan).

To analyze the extent of cell death caused by various VdTRP mutant proteins, 100 µL purified mutant proteins including His-GST-TRP, His-GST, His-GST-TRP$^{1-75}$, His-GST-TRP$^{1-92}$, His-GST-TRP$^{1-112}$, His-GST-TRP$^{1-132}$, His-GST-TRP$^{1-152}$, His-GST-TRP$^{(P/A)}$ and His-GST-TRP$^{\triangle CFEM}$ were respectively added to separate preparations of 100 µL protoplast solutions. The solution was cultured at room temperature in a shaker (10 rpm) for 3 h, then they were placed on a concave slide and submitted to observation under the microscope (BX51 Olympus, Japan), taking pictures and counting the number of surviving protoplast cells.

Subcellular localization and BiFC assays

The recombinant plasmids were transformed into *Agrobacterium tumefaciens* and suspended in MES buffer. Three days after *N. benthamiana* injection, different fluorescence signals from GFP, RFP, or YFP were detected using the confocal laser scanning microscope (SP8 Lecia, Germany), respectively. Plasma membrane-localized aquaporins AtPIP2A[62] and nuclear localization proteins histone B2 AtHTB2[63] were selected as positive controls.

Protein–lipid binding assay

The coding region of VdTRP without signal peptide was inserted in the *pCold-GST* vector, and was expressed in *E. coli*. The purified protein was used to perform lipid binding assay following the protocol described by Liu et al.[64]. To prevent nonspecific binding, lipid strips (Echelon Biosciences) were pre-incubated with the binding assay buffer (3% BSA in TBST) for 1 h at room temperature. Next the lipid strips were incubated overnight at 4 °C in TBST buffer containing 10 µg/mL protein (0.3% BSA). After washing 3 times with TBST buffer, His antibody was added and incubated at room temperature for 2 h. Following another 3 washes with TBST buffer, the horse-radish-peroxidase-

conjugated secondary antibody was added and incubated for 1 h at room temperature. The proteins were visualized using a chemiluminescence ECL kit (Vazyme) after washing 3 times with TBST buffer.

SICM topography and extracellular surface charge mapping

The H9c2 cell line of rat cardiomyocyte is from American Type Culture Collection (ATCC). Cell culture is based on the method as described by Liu et al. [65]. Once the cell is prepared, 80 μL of PBS, and purified proteins His-GST and His-GST-TRP (1 mg/mL) were separately added to H9c2 cell line culture dishes. After incubation at room temperature for 2 min, the supernatant was discarded and 1.5 mL of serum-free cell culture medium was added to culture dishes. The impact of VdTRP protein on cell morphology was first observed using an optical microscope (NIB610-FL Nexcope, USA). Then cell surface topography and surface charge variation were analyzed by scanning ion conductance microscopy (SICM, N12 Park, Korea), as reported previously[28].

For SICM scanning, nanopipette of ≈70 nm in diameter was used. The topographic and current images were obtained using skip and approach-retract scan dual modes described by Song et al. [28]. In this method, the nanopipette tip approaches the sample surface from an initial position $D_{ps\text{-}max}$ (D_{ps}, distance between scanning probe and sample surface), and stops at $D_{ps\text{-}min}$ when the current reduction exceeds a predefined set point (usually 2%). After reaching $D_{ps\text{-}min}$, the ionic current is measured and linked with position information. Subsequently, the nanopipette withdraws from $D_{ps\text{-}min}$ and returns to $D_{ps\text{-}max}$. In addition to maintaining a constant approach speed and a 2% current reduction as the setpoint, the approach step includes a 1% mid setpoint. At this mid-setpoint, the nanopipette is slightly raised and then continues approaching the sample at half of the original speed. ΔI indicate the absolute value of current difference between $D_{ps\text{-}min}$ and $D_{ps\text{-}max}$ in each approach/withdraw cycle and used for surface charge map construction.

During morphology detection, the ΔI-based SICM system performs a coarse scan (64 × 32 pixels) and a fine scan (256 × 128 pixels) in a 40 × 20 μm^2 area within 20 min. For probing the topography and charge distribution of cellular membrane, the system performs a coarse scan (32 × 32 pixels) and a fine scan (128 × 128 pixels) in a 5 × 5 μm^2 area in ≈8 min. During the scanning process, the oscilloscope captures time traces of z-piezoelectric movement and ion current, which were used for constructing ΔI images and for further analyses. Data analysis was carried out using XEI (Park Systems), LabVIEW, and Origin2019b (Origin Lab Corp.). Ionic current images were constructed using LabVIEW programs, while the 3D and 2D topography images were analyzed using XEI[28].

Extraction of total plant protein and apoplastic protein

Plant protein extraction kit (BC3720 Soarbio) was used to extract total protein. The amount of 0.2 g of plant leaves was sampled and crushed in liquid nitrogen environment, a total of 1 mL lysate (10 μL protease inhibitor and 10 μL PMSF) was added, cleaved at 4 °C for 20 minutes, centrifuged at high speed. The supernatant was collected as the total protein.

For apoplastic protein extraction, the leaves were completely immersed in the PBS solution and a high-pressure vacuum pump (0.75 kPa) was used to ensure that the PBS solution was fully pressed into the leaves. Subsequently, the leaves were placed in a 50 mL centrifuge tube and centrifuged at 1000 × *g* for 5 min at 4 °C to obtain apoplastic protein[66].

Phylogenetic tree construction

The IPGGCNPAHPGSCP conserved fragment was blasted with the multi-species protein sequence from NCBI, and some representative fungal protein sequences were selected. These sequences were aligned using MEGA X, and a phylogenetic tree was constructed using the maximum likelihood method[67].

Yeast two-hybrid screen and validation

VdTRP was employed as the bait protein. The BD-VdTRP plasmids, cotton cDNA library and the linearized AD-rec vector were co-transformed into yeast using the Y2H screening technique, and positive clones were screened on SD/-Trp-Leu-His medium. Then these clones were re-plated on SD/-Trp-Leu-His-Ade medium for further stringent selection.

Luciferase complementation assay

The recombinant plasmids were constructed on *pCambia1300-cLuc* and *pCambia1300-nLuc* vectors, transformed into *Agrobacterium tumefaciens*, and resuspended in MES buffer. Luc fluorescence was observed three days after *N. benthamiana* leaves injection.

Co-immunoprecipitation assays

The recombinant plasmids were constructed on *pCambia1390-3×FLAG* and *p2YC-HA* vectors, transformed into *Agrobacterium tumefaciens*, and resuspended in MES buffer. Three days after *N. benthamiana* leaves injection, total protein was extracted, incubated with FLAG beads, and eluted proteins were analyzed by immunoblotting with FLAG and HA antibodies.

In vitro GST pull-down assay

GST-CTL1 (without signal peptide), His-VdTRP (without signal peptide), and His-TRP$^{\triangle 153\text{-}196}$ (without signal peptide and C-terminal) were induced and expressed in *E. coli* strain *Rossetta2* (DE3). For in vitro protein interaction assay, the His protein was pulled down using GST beads. Immunoblotting detection was carried out using GST and His antibodies.

Microscale thermophoresis (MST) assays

The MST assay was utilized to assess the binding affinity between TRP and CTL1. Purified proteins His-GST-TRP (without signal peptide) and His-GST-TRP$^{\triangle 153\text{-}196}$ (without signal peptide and C-terminal) were labeled with 200 nM in PBST buffer for 30 min as the kit instructions (Monolith His-Tag Labeling Kit RED-tris-NTA 2nd Generation, MO-L018). The labeled protein was then combined with gradient dilutions of GST-CTL1 (without signal peptide) and GST proteins, and incubated at room temperature for 30 min. Samples were loaded into the capillary (Monolith Series Premium Capillaries, MO-K025) and analyzed using a Monolish NT.115 device. The raw data were subsequently processed using MO Affinity Analysis software (V2.2.4).

Chitinase enzyme activity assay

The recombinant plasmids were individually constructed on *pBIN-GFP4* vector, transformed into *Agrobacterium tumefaciens*, and resuspended in MES buffer. Three days later, the total proteins of *N. benthamiana* without *Agrobacterium* injection, the control GFP, and the CTL1-GFP were extracted. Chitinase enzyme activity was measured using a chitinase activity kit (Jiancheng biology of Nanjing, A139-1-1) and visible spectrophotometry. Chitinase hydrolyzes chitin into N-acetylglucosamine, which is then coupled with DNS to produce a red molecule with a distinctive absorption peak at 540 nm, and the rate of rise in absorbance represents chitinase activity.

In vitro antifungal test of *V. dahliae*

The amount of 100 μL of *V. dahliae* solution was added to the PDA and spread evenly. Next, 3 sterile filter paper pieces with a diameter of 1 cm were placed on the PDA medium. Subsequently, the amount of 200 μL of purified GST protein (1 μg/μL), CTL1-GST (without signal peptide) protein (1 μg/μL) and water were added onto the different filter paper pieces. The PDA was then cultured at 25 °C for 5 days, investigated and photographed.

VIGS experiments

The cotton *CTL1* gene-specific fragment was inserted into the *TRV2* vector. Empty vectors TRV:00 and TRV:*CLA1* (cloroplastos alterados 1) were used as negative and positive controls, respectively. The plasmids were transformed into *Agrobacterium tumefaciens* and injected into the cotyledons of 7-day-old cotton seedlings. Two weeks after injection, the expression of target genes was detected in experimental plants and controls.

Cell section observation

Cotton tissues were sequentially dehydrated with 20–50–70–100% ethanol, and then embedded in resin. Ultrathin resin slices with a thickness of 2 μm were cut with a microtome, stained with Safranine O-Fast Green Staining, and observed and photographed with a microscope (BX51 Olympus, Japan).

Measurement of cotton roots morphology

Cotton roots were photographed using a root scanner (i800plus; Zhejiang TOP Cloud-agri Technology Co., Ltd.). The root system analysis software (LA-S; WSeen) was applied to analyze the image and obtain the specific shape data of the cotton roots[68].

Determination of sucrose, fructose, and glucose content

Carbohydrate analysis was performed following Wang et al. [22]. A mount of 0.2 g of cotton stem tissues was ground into powders in liquid nitrogen. Firstly, the samples were extracted with 4 mL of preheated 80% ethanol at 80 °C for 5 min, then the mixture was cooled and centrifuged at high speed to collect the supernatant. Secondly, the precipitates were resuspended in 2 mL of 50% ethanol to collect the supernatant as described above. Thirdly, the precipitates were resuspended in 2 mL of ddH_2O and the solution was kept at boiling water for 10 min. The samples were centrifuged again as described above and supernatant was recollected. The supernatants collected were mixed with an equal volume of chloroform and shaken vigorously. The aqueous phase was collected, dried in a vacuum and re-dissolved in 1 mL 50% acetonitrile (acetonitrile: water =50:50). The samples were filtrated with 0.45 μm filter membrane and detected using an ultra-high performance liquid chromatograph system (ACQUITY H-Class, Waters, Massachusetts, USA). At least 5 samples per cotton line were measured, each containing at least 3 plants.

Determination of cellulose content

The cellulose content was measured by visible spectrophotometry using a cellulose content detection kit (BC4280, Solarbio). Approximately 5 mg of dried cell wall materials of cotton tissues was sampled, 0.5 mL of distilled water and 0.75 mL of concentrated sulfuric acid was added to the sample, then mix and ice-bath for 30 min. The supernatant was collected by centrifuging at high speed and diluted 20 times for testing. The cellulose was heated and degraded into β-D-glucose under acidic circumstances, and the cellulose content was measured by utilizing anthrone chromogen under high acid conditions.

Determination of SA content

SA content was measured following Guo et al. [39]. A mount of 0.1 g of cotton root tissues was ground into powders in liquid nitrogen, and 750 μL of extraction buffer (methanol: water: glacial acetic acid 80: 19: 1) was added and shaken at low temperature for 12 h. The supernatant was collected by centrifuging at high speed. Then, the precipitates were resuspended in 250 μL of extraction buffer at low temperature for 2 h. The supernatant was collected as described above and mixed with the previous supernatant. The supernatants were freeze-dried, and 300 μL methanol solution was added to the sample to re-dissolve. The SA content was detected using the Lliquid Dhromatography Coupled to Triple Quadrupole Mass Spectrometryto (Triple Quad 6500+, AB Siex). At least 6 samples per cotton line were measured, each containing at least 3 plants.

Targeted determination of sugar and aldehydes

A mount of 40 mg of ground cotton root tissues and 100 μL of methanol were mixed into a centrifuge tube. The mixture was vortexed for 30 s, then centrifuged at 15,000 × *g* for 15 min at 4 °C. The supernatant of 60 μL was collected and freeze-dried. Next, 40 μL methoxyaminopyridine hydrochloride solution (20 μg/mL) was added to the sample to re-dissolve and react at 37 °C for 90 min. Afterward, 40 μL BSTFA (containing 1% TMCS) was added and reacted at 70 °C for 60 min. Finally, the mixture was cooled at room temperature for GC-MS analysis (Agilent, 7890A/5975C, CA, USA). At least 6 samples per cotton line were measured, each containing at least 3 plants.

Investigation of cotton fiber quality traits and yield components

Cotton plants were cultivated in the experimental base of Nanjing Agricultural University at Ledong, Hainan province (108°E, 18°N). Boll number of transgenic lines OE138, OE172 and control W0 were counted during the cotton boll opening stage. A total of 25 bolls from the middle branches of each accession were sampled to weigh the lint and seeds and calculate the yield components. The fiber quality traits were measured by the Center of Cotton Fiber Quality Inspection and Testing of the Ministry of Agriculture and Rural Affairs (Anyang, China). The data were generated with three biological replicates.

Statistics & reproducibility

Statistical significance was assessed by one-way ANOVA with Duncan's multiple range test (the *p*-values are provided in the Source data) or two-tailed Student's *t* test (the *p*-values are provided in the figures). All analyses were performed by SPSS (SPSS 27.0.0; SPSS, Chicago, IL, USA).

Reporting summary

Further information on research design is available in the Nature Portfolio Reporting Summary linked to this article.

Data availability

All data generated from this study are available in the article and Supplementary Information files. The RNA-seq data from this study have been deposited in the National Center for Biotechnology Information Sequence Read Archive under accession number PRJNA904494. The primers used in this study are listed in Supplementary Data 5. Source data are provided with this paper.

References

1. Stukenbrock, E. & Gurr, S. Address the growing urgency of fungal disease in crops. *Nature* **617**, 31–34 (2023).
2. Lo Presti, L. et al. Fungal effectors and plant susceptibility. *Annu. Rev. Plant Biol.* **66**, 513–545 (2015).
3. Tariqjaveed, M. et al. Versatile effectors of phytopathogenic fungi target host immunity. *J. Integr. Plant Biol.* **63**, 1856–1873 (2021).
4. de Jonge, R. Conserved fungal LysM effector Ecp6 prevents chitin-triggered immunity in plants. *Science* **329**, 953–955 (2010).
5. Wang, Y., Pruitt, R. N., Nürnberger, T. & Wang, Y. Evasion of plant immunity by microbial pathogens. *Nat. Rev. Microbiol.* **20**, 449–464 (2022).
6. Kale, S. D. et al. External lipid PI3P mediates entry of eukaryotic pathogen effectors into plant and animal host cells. *Cell* **142**, 284–295 (2010).
7. Whisson, S. C. et al. A translocation signal for delivery of oomycete effector proteins into host plant cells. *Nature* **450**, 115–118 (2007).
8. Dou, D. & Zhou, J. M. Phytopathogen effectors subverting host immunity: different foes, similar battleground. *Cell Host Microbe* **12**, 484–495 (2012).

9. Jones, J. D. G. & Dangl, J. L. The plant immune system. *Nature* **444**, 323–329 (2006).
10. Kourelis, J. & van der Hoorn, R. A. L. Defended to the nines: 25 years of resistance gene cloning identifies nine mechanisms for R protein function. *Plant Cell* **30**, 285–299 (2018).
11. Bacete, L., Mélida, H., Miedes, E. & Molina, A. Plant cell wall-mediated immunity: cell wall changes trigger disease resistance responses. *Plant J.* **93**, 614–636 (2018).
12. Jian, Y. et al. How plants manage pathogen infection. *EMBO Rep.* **25**, 31–44 (2023).
13. Lorang, J. M., Sweat, T. A. & Wolpert, T. J. Plant disease susceptibility conferred by a "resistance" gene. *Proc. Natl Acad. Sci. USA* **104**, 14861–14866 (2007).
14. Faris, J. D. et al. A unique wheat disease resistance-like gene governs effector-triggered susceptibility to necrotrophic pathogens. *Proc. Natl Acad. Sci. USA* **107**, 13544–13549 (2010).
15. Johal, G. S. & Briggs, S. P. Reductase activity encoded by the *HM1* disease resistance gene in maize. *Science* **258**, 985–987 (1992).
16. Wang, H. et al. Horizontal gene transfer of *Fhb7* from fungus underlies *Fusarium* head blight resistance in wheat. *Science* **368**, eaba5435 (2020).
17. Vleeshouwers, V. G. A. A. & Oliver, R. P. Effectors as tools in disease resistance breeding against biotrophic, hemibiotrophic, and necrotrophic plant pathogens. *Mol. Plant-Microbe Interact.* **27**, 196–206 (2014).
18. Li, Q., Wang, B., Yu, J. & Dou, D. Pathogen-informed breeding for crop disease resistance. *J. Integr. Plant Biol.* **63**, 305–311 (2021).
19. Vleeshouwers, V. G. et al. Effector genomics accelerates discovery and functional profiling of potato disease resistance and phytophthora infestans avirulence genes. *PLos One* **3**, e2875 (2008).
20. Zaidi, S. S., Mukhtar, M. S. & Mansoor, S. Genome editing: targeting susceptibility genes for plant disease resistance. *Trends Biotechnol.* **36**, 898–906 (2018).
21. Römer, P., Recht, S. & Lahaye, T. A single plant resistance gene promoter engineered to recognize multiple TAL effectors from disparate pathogens. *Proc. Natl Acad. Sci. USA* **106**, 20526–20531 (2009).
22. Wang, G. et al. Cotton peroxisome-localized lysophospholipase counteracts the toxic effects of *Verticillium dahliae* NLP1 and confers wilt resistance. *Plant J.* **115**, 452–469 (2023).
23. Dangl, J. L. et al. Comparative genomics yields insights into niche adaptation of plant vascular wilt pathogens. *PLoS Pathog.* **7**, e1002137 (2011).
24. Zhou, B. J., Jia, P. S., Gao, F. & Guo, H. S. Molecular characterization and functional analysis of a necrosis- and ethylene-inducing, protein-encoding gene family from *Verticillium dahliae*. *Mol. Plant-Microbe Interact.* **25**, 964–975 (2012).
25. Santhanam, P. et al. Evidence for functional diversification within a fungal NEP1-like protein family. *Mol. Plant-Microbe Interact.* **26**, 278–286 (2013).
26. Kou, Y., Tan, Y. H., Ramanujam, R. & Naqvi, N. I. Structure–function analyses of the Pth11 receptor reveal an important role for CFEM motif and redox regulation in rice blast. *N. Phytologist* **214**, 330–342 (2016).
27. Liu, Z., Jian, Y. & Shan, L. Disarm resistance: Fungal effectors target WAK alternative splicing variant for virulence. *Cell Rep.* **42**, 111939 (2023).
28. Song, Y. et al. Imaging structural and electrical changes of aging cells using scanning ion conductance microscopy. *Small Methods* **2023**, 2301315 (2023).
29. Sánchez-Rodríguez, C. et al. CHITINASE-LIKE1/POM-POM1 and its homolog CTL2 are glucan-interacting proteins important for cellulose biosynthesis in *Arabidopsis*. *Plant Cell* **24**, 589–607 (2012).
30. Peraro, M. D. & van der Goot, F. G. Pore-forming toxins: ancient, but never really out of fashion. *Nat. Rev. Microbiol.* **14**, 77–92 (2015).
31. Pircl, K. et al. An oomycete NLP cytolysin forms transient small pores in lipid membranes. *Sci. Adv.* **8**, 9406 (2022).
32. Hermans, C., Porco, S., Verbruggen, N. & Bush, D. R. Chitinase-like protein CTL1 plays a role in altering root system architecture in response to multiple environmental conditions. *Plant Physiol.* **152**, 904–917 (2010).
33. Wu, B. et al. Brittle culm15 encodes a membrane-associated Chitinase-like protein required for cellulose biosynthesis in rice. *Plant Physiol.* **159**, 1440–1452 (2012).
34. Jiao, S. et al. Chitinase-like1 plays a role in stalk tensile strength in *Maize*. *Plant Physiol.* **181**, 1127–1147 (2019).
35. Zhong, R., Lee, C., Zhou, J., McCarthy, R. L. & Ye, Z. H. A battery of transcription factors involved in the regulation of secondary cell wall biosynthesis in *Arabidopsis*. *Plant Cell* **20**, 2763–2782 (2008).
36. Taylor-Teeples, M. et al. An *Arabidopsis* gene regulatory network for secondary cell wall synthesis. *Nature* **517**, 571–575 (2015).
37. Smit, M. E. et al. A PXY-mediated transcriptional network integrates signaling mechanisms to control vascular development in *Arabidopsis*. *Plant Cell* **32**, 319–335 (2020).
38. Hussey, S. G., Mizrachi, E., Creux, N. M. & Myburg, A. A. Navigating the transcriptional roadmap regulating plant secondary cell wall deposition. *Front. Plant Sci.* **4**, 325 (2013).
39. Guo, Z. et al. Two cotton isochorismate synthase genes are biased functionally in regulating salicylic acid and phylloquinone biosynthesis. *Environ. Exp. Bot.* **216**, 105540 (2023).
40. Lee, K. P. et al. PLANT NATRIURETIC PEPTIDE A and its putative receptor PNP-R2 antagonize salicylic acid-mediated signaling and cell death. *Plant Cell* **32**, 2237–2250 (2020).
41. Yang, J. et al. Identification of cell wall-associated kinases as important regulators involved in *Gossypium hirsutum* resistance to *V. dahliae*. *BMC Plant Biol.* **21**, 220 (2021).
42. Wang, X., Zafian, P., Choudhary, M. & Lawton, M. The PR5K receptor protein kinase from *Arabidopsis thaliana* is structurally related to a family of plant defense proteins. *Proc. Natl Acad. Sci. USA* **93**, 2598–2602 (1996).
43. Klosterman, S. J., Atallah, Z. K., Vallad, G. E. & Subbarao, K. V. Diversity, Pathogenicity, and management of *Verticillium* species. *Annu. Rev. Phytopathol.* **47**, 39–62 (2009).
44. Yang, C. L. et al. Cotton major latex protein 28 functions as a positive regulator of the ethylene responsive factor 6 in defense against *Verticillium dahliae*. *Mol. Plant* **8**, 399–411 (2015).
45. Zhang, Z. N. et al. Systematic analyses reveal uniqueness and origin of the CFEM domain in fungi. *Sci. Rep.* **5**, 13032 (2015).
46. Yeung, T. et al. Membrane phosphatidylserine regulates surface charge and protein localization. *Science* **319**, 210–213 (2008).
47. Wang, D. et al. *Verticillium dahliae* CFEM proteins manipulate host immunity and differentially contribute to virulence. *BMC Biol.* **20**, 55 (2022).
48. Zuo, N. et al. Fungal CFEM effectors negatively regulate a maize wall-associated kinase by interacting with its alternatively spliced variant to dampen resistance. *Cell Rep.* **41**, 111877 (2022).
49. Mesarich, C. H., Bowen, J. K., Hamiaux, C. & Templeton, M. D. Repeat-containing protein effectors of plant-associated organisms. *Front. Plant Sci.* **6**, 872 (2015).
50. Ma, L. S., Pellegrin, C. & Kahmann, R. Repeat-containing effectors of filamentous pathogens and symbionts. *Curr. Opin. Microbiol.* **46**, 123–130 (2018).
51. Williamson, M. P. The structure and function of proline-rich regions in proteins. *Biochemical J.* **297**, 249–260 (1994).
52. Ren, X. & Hurley, J. H. Proline-rich regions and motifs in trafficking: from ESCRT interaction to viral exploitation. *Traffic* **12**, 1282–1290 (2011).
53. Hurley, J. H. & Hanson, P. I. Membrane budding and scission by the ESCRT machinery: it's all in the neck. *Nat. Rev. Mol. Cell Biol.* **11**, 556–566 (2010).

54. Gendler, S. J. et al. Molecular cloning and expression of human tumor-associated polymorphic epithelial mucin. *J. Biol. Chem.* **265**, 15286–15293 (1990).
55. Almagro Armenteros, J. J. et al. SignalP 5.0 improves signal peptide predictions using deep neural networks. *Nat. Biotechnol.* **37**, 420–423 (2019).
56. Waterhouse, A. et al. SWISS-MODEL: homology modelling of protein structures and complexes. *Nucleic Acids Res.* **46**, W296–W303 (2018).
57. Mirdita, M. et al. ColabFold: making protein folding accessible to all. *Nat. Methods* **19**, 679–682 (2022).
58. Letunic, I., Khedkar, S. & Bork, P. SMART: recent updates, new developments and status in 2020. *Nucleic Acids Res.* **49**, D458–D460 (2021).
59. Li, F. et al. Agrobacterium mediated co-transformation of multiple genes in upland cotton. *Plant Cell Tissue Organ Cult.* **97**, 225–235 (2009).
60. Xu, J. et al. Host-induced gene silencing of a regulator of G protein signaling gene (VdRGS1) confers resistance to *Verticillium* wilt in cotton. *Plant Biotechnol. J.* **16**, 1629–1643 (2018).
61. Wang, Z. et al. Recognition of glycoside hydrolase 12 proteins by the immune receptor RXEG1 confers *Fusarium* head blight resistance in wheat. *Plant Biotechnol. J.* **4**, 769–781 (2023).
62. Qiu, J., McGaughey, S. A., Groszmann, M., Tyerman, S. D. & Byrt, C. S. Phosphorylation influences water and ion channel function of AtPIP2;1. *Plant, Cell Environ.* **43**, 2428–2442 (2020).
63. Zhang, L. et al. Gateway-compatible vectors for functional analysis of proteins in cell type specific manner. *Plant Methods* **16**, 93 (2020).
64. Liu, X. et al. Inflammasome-activated gasdermin D causes pyroptosis by forming membrane pores. *Nature* **535**, 153–158 (2016).
65. Liu, Y. et al. Cardioprotective roles of β-hydroxybutyrate against doxorubicin induced cardiotoxicity. *Front. Pharmacol.* **11**, 603596 (2021).
66. Xia, Y. et al. N-glycosylation shields *Phytophthora sojae* apoplastic effector PsXEG1 from a specific host aspartic protease. *Proc. Natl Acad. Sci. USA* **117**, 27685–27693 (2020).
67. Kumar, S., Stecher, G., Li, M., Knyaz, C. & Tamura, K. MEGA X: Molecular evolutionary genetics analysis across computing platforms. *Mol. Biol. Evolution* **35**, 1547–1549 (2018).
68. Huang, Y. et al. Improving rice nitrogen-use efficiency by modulating a novel monouniquitination machinery for optimal root plasticity response to nitrogen. *Nat. Plants* **9**, 1902–1914 (2023).

Acknowledgements

We are grateful to Dr. Feng Chen and Ms. Yao Song from Nanjing Medical University for kind help in SICM related experiments. Many thanks to Profs. Yan Wang, Daolong Dou, Shan Li, Dawei Guo and Qun Zhang from Nanjing Agricultural University for their professional suggestions and assistances to improve the manuscript. We also thank the Bioinformatics Center of Nanjing Agricultural University for providing the data analysis platform. This work was financially supported in part by grants from Biological Breeding-National Science and Technology Major Project (2023ZD04070 to W.G.), Jiangsu Key R & D Program (BE2022384 to W.G.), and the Collaborative Innovation Center for Modern Crop Production co-sponsored by Province and Ministry (CIC-MCP) (No. 10 to W.G.).

Author contributions

W.G., X.W., and H.L. designed research; H.L., W.Z., Q.H., G.W., R.A., H. X., Z.G. and L.W. performed research; H.L., W.L., X.W., and W.G. analyzed data; X.W., H.L., and W.G. wrote the paper, W.G. and X.W. revised the paper.

Competing interests

The authors declare no competing interests.

Additional information

Supplementary information The online version contains supplementary material available at https://doi.org/10.1038/s41467-024-54470-0.

Correspondence and requests for materials should be addressed to Xinyu Wang or Wangzhen Guo.

Peer review information *Nature Communications* thanks Fei Li, and the other, anonymous, reviewer(s) for their contribution to the peer review of this work. A peer review file is available.